Doctoral Thesis

Non-linear Optical Microscopy and Spectroscopy for Biomedical Studies

Stina Guldbrand

UNIVERSITY OF GOTHENBURG

Department of Physics
University of Gothenburg
SE-412 96 Göteborg, Sweden 2012

Non-linear Optical Microscopy and Spectroscopy for Biomedical Studies
STINA GULDBRAND
ISBN: 978-91-628-8599-1

Doktorsavhandling vid Göteborgs universitet

Department of Physics
University of Gothenburg
SE-412 96 Göteborg
Sweden
Telephone +46 (0)31 786 0000

Typeset in LaTeX

Figures created using MATLAB and Power Point

Till Erik, Ella, Majken

My beloved and neglected nephew and nieces.

Non-linear Microscopy and Spectroscopy for Biomedical Studies

This thesis is based on the application of non-linear optical microscopy and spectroscopy techniques within biomedical research. Non-linear optical microscopy gives the possibility of exciting fluorophores using near infrared light. This is an advantage when working with biological tissue, which has low absorption in this wavelength area, making up an "open window" for non-invasive three dimensional imaging. Of particular interest has been the study of fluorescent xenobiotics in human skin using two-photon fluorescence laser scanning microscopy. The background is the desire to develop new non-invasive tools to study topical drug delivery and improve the understanding of mechanisms involved in contact allergy. In addition, two-photon fluorescence microscopy is a potential tool for non-invasive skin cancer diagnostics, which also is a topic of this thesis.

In order to acquire quantitative data, two-photon fluorescence microscopy has been combined with fluorescence correlation spectroscopy (TPFCS). This is to the best of my knowledge the first time TPFCS has been applied to study the diffusion and distribution of fluorescent molecules in human skin.By the use of this method a reactive compound, acting as a contact allergen, has been demonstrated to bind to proteins in the top epidermal layers of the skin, resulting in a significantly slower diffusion.

It has been proposed that endogenously formed protoporphyrin IX (PpIX) can be applied to improve contrast when performing two-photon fluorescence microscopy for diagnostics of non-melanoma skin cancer. In this thesis, it is demonstrated that detection of two-photon excited fluorescence of endogenous PpIX in human skin is not possible. Instead, it is preferable to use a slightly shorter wavelength, i.e. 710 nm, to induce one-photon anti-Stokes fluorescence. This finding is of great importance for continued work in the field, bringing non-linear optical microscopy into the clinics.

Plasmonic noble metal nanoparticles, e.g. gold nanoparticles, have been proposed as contrast enhancers for several biomedical applications. In this thesis, gold nanoparticles have been explored with respect to their multiphoton induced luminescence when combined with non-linear optical microscopy. By investigating 10 nm gold nanoparticles deposited on glass plates, it is here demonstrated that aggregation and short inter-particle distances are prerequisites in order to detect multiphoton induced luminescence. Thus detection of single particles in a biological environment is unlikely, and future work should be undertaken to explore how the clustering can be controlled in a biological environment to, e.g, be used as a contrast mechanism.

Keywords: Two-Photon Excitation Microscopy, Fluorescence Correlation Spectroscopy, Multiphoton Luminescence, Human Skin, Gold nanoparticles

Research Publications

The work presented in this thesis is based upon four research articles, referred to as Paper I, II, III and IV.

Paper I

Two-photon fluorescence correlation spectroscopy combined with measurements of point spread function; investigations made in human skin
S.Guldbrand, C.Simonsson, M.Goksör, M.Smedh and M.B.Ericson
Optics Express, 18:15289 – 15302, 2010
selected for publication in Virtual Journal for Biomedical Optics (2010)

Paper II

Two-photon fluorescence correlation spectroscopy as a tool for measuring molecular diffusion within human skin
S.Guldbrand, V.Kirejev, C.Simonsson, M.Goksör, M.Smedh and M.B.Ericson
European Journal of Pharmaceutics and Biopharmaceutics, accepted in October, 2012

Paper III

Anti-Stokes fluorescence from endogenously formed Protoporphyrin IX – Implications for clinical multiphoton diagnostics
D.Kantere*, S.Guldbrand*, J.Paoli, M.Goksör, D.Hanstorp, A.-M. Wennberg, M.Smedh and M.B.Ericson
* Both authors have contributed equally to this study
Journal of Biophotonics, accepted in August 2012

Paper IV

Multiphoton induced luminescence from 10 nm gold nanoparticles – the effect of inter-particle distance and aggregation
S.Guldbrand, H.Evenbratt, J.Borglin, V.Kirejev and M.B.Ericson
In Manuscript

My contribution to the publications:

Paper I

I planned the study together with Smedh and Ericson. I performed all the experiments and the data analysis. I am the main author of the paper.

Paper II

I planned the study together with Smedh and Ericson. I performed all the experiments and the data analysis. I am the main author of the paper.

Paper III

I performed the measurements on PpIX in solution. I did the microscopy experiments on skin together with Kantere. I analysed the data together with Kantere, Smedh and Ericson. I performed the calculations and analysis of the probability for Anti-Stokes excitation. I wrote the paper together with Kantere and Ericson.

Paper IV

I planned the study together with Evenbratt and Ericson. I performed the microscopy experiments together with Evenbratt. I performed the MatLab analysis. I am the main author together with Ericson.

Papers not included in this thesis

Multiphoton microscopy – a powerful tool in skin research and topical drug delivery science
V.Kirejev, S.Guldbrand, J.Borglin, C.Simonsson and M.B.Ericson
Journal of Drug Delivery Science and Technology, 2012, **22** (3), 250 – 259
My contribution to this review paper is covered in paper I and II

Measuring the diffusion of fluorophores in human skin by two-photon fluorescence spectroscopy combined iwth measurements of point spread function
S.Guldbrand, C.Simonsson, M.Goksör, M.Smedh and M.B.Ericson
Proceedings of SPIE, 2011, **7903**, 790329
My contribution to this paper is covered in paper I and II

Novel nanocarriers for topical drug delivery: Investigation delivery efficiency and distribution in skin using two-photon microscopy
V.Kirejev, S.Guldbrand, B.Bauer, M.Smedh and M.B.Ericson
Proceedings of SPIE, 2011, **7903**, 79032S
My contribution to this paper is minor

Point-spread function measured in human skin using two-photon fluorescence microscopy
M.B.Ericson, C.Simonsson, S.Guldbrand, C.Ljungblad, J.Paoli and M.Smedh
Proceedings of SPIE, 2009, **7367**, 73671R
My contribution to this paper is covered in paper I and II

Two-photon laser-scanning fluorescence microscopy applied for studies of human skin
M.B.Ericson, C.Simonsson, S.Guldbrand, C.Ljungblad, J.Paoli and M.Smedh
Journal of Biophotonics, 2008 **1** (4) 320 – 330
My contribution to this paper is minor

Abbrevations

ALA	aminolevulinic acide
AOM	acousto-optic modulator
APD	avalanche photodiode
APDES	(3-Aminopropyl)-diethyoxysilane
AuNPs	gold nanoparticles
CARS	Coherent anti-stokes raman scattering
CCD	Charge-coupled device
CLSM	Confocal laser scanning microscopy
FCS	Fluorescence correlation spectroscopy
FLIM	Fluorescent lifetime imaging microscopy
FWHM	Full width at half maximum
MAL	methylaminolevulinate
MIL	Multiphoton induced luminescence
NA	Numerical aperture
NIR	Near infrared
PDT	Photodynamic therapy
PMT	Photomultiplier tube
PpIX	Protoporphyrin IX
PSF	Point spread function
RB	Rhodamine B
RBITC	Rhodamine B isothiocyanate
SHG	Second harmonic generation
SRB	Sulforhodamine B
TCSPC	Time-correlated single-photon counting
Ti:Sapphire	Titanium Sapphire
TP	Two-photon
TPLSM	Two-photon excitation laser scanning microscopy
TPFCS	Two-photon excitation laser scanning microscopy fluorescence correlation spectroscopy
wd	working distance

Symbols

C	concentration
D	diffusion
D_o	diameter of a small opening
ϵ	Molar extinction coefficient
J	flux
k	Boltzmanns constant
μ	Chemical potential
n	refractive index
λ	wavelength
N	average number of molecules within the focal volume
ω	Frequency
Q	Fluorescence quantum yield
R	Molar gas constant
R_h	Hydrodynamic radius
σ	Absorption cross section
S	Entropy
τ_D	diffusion time

Contents

Chapter 1

Introduction

Why use non-linear optics for biomedical studies? The answer is not ”because we can”, but because non-linear optics enables stretching of the resolution limit in high-scattering materials, and gives a chance to investigate inherent processes without destroying the sample.

The first theoretical report of two-photon excitation came as early as 1931, when Maria Göppert-Mayer described the theory behind the process [1, 2]. At that point, it was not possible to test her theory, as this requires a monochromatic light source with high intensity. Thirty years later, the newly invented laser solved this problem, and two-photon excitation could be verified in reality [3]. The high intensity is needed as the likelihood of two photon being absorbed simultaneously is small. The probability of observing a two-photon absorption event on a bright sunny day is 1 per 10,000,000 years, whereas the one-photon absorption takes place every second [4]. The trick to achieving high intensity without cranking up the laser to eleven[1] is to use a pulsed laser. The output from this laser is a train of pulses where each pulse has a high power (kW), but the average power remains at a moderate value (mW). A continuous laser beam with an output power in the kW range would be risky, expensive, and inappropriate for biological applications.

The use of the two-photon excitation process in microscopy was first reported in 1990, by Denk *et al.*, who did experiments on fluorescent beads and on cells [5]. As excitation by two photons allows working in the near infrared (NIR) area, the technique is well suited for optically dense biological tissue [6, 7, 8, 9], such as human skin. The main advantage compared to confocal scanning microscopy (which is based on one-photon excitation) is the enhanced penetration depth. This is an effect of the low probability of the excitation process in combination with the lower absorption coefficient of the NIR light. Two-photon excitation laser scanning microscopy (TPLSM) has been used for imaging of normal skin [10, 11, 12], to study transdermal drug delivery [13, 14] and for clinical studies of skin cancer [15, 16].

[1] A term coined in the movie *This Is Spinal Tap* where the guitarist proudly demonstrates a top-of-the-line amplifier with the highest volume step labelled 'eleven' instead of the more usual 'ten'.

The information from a microscope is provided as a snapshot. It tells the viewer what the object looked like in a specific moment, but quantitative information is lacking. To acquire this information, fluorescence correlation spectroscopy (FCS) can be used. This is a method where the measured signal is analysed with respect to itself at a later time. It is used for analysing the diffusion and the number of large molecules at low concentrations, and is often used in biological environments. In this thesis, the combination of FCS and TPLSM is used for the first time for quantitative measurements in human skin, revealing specific information about the molecular dynamics within skin which has not previously been available. Future possible applications include the optimisation of topical drug delivery and the investigation of allergen-protein formation. Diffusion plays a major role in this context, and so it is important to develop a trustworthy method for these measurements.

Recently, TPLSM has been reported to be used in the clinics for detecting non-melanoma skin cancer, although the research is based on preliminary data [17, 18]. The work presented in this thesis shows that a small shift in excitation wavelength makes a great difference to the outcome. This result is of great importance to ensure an effective and reliable method to use on patients with non-melanoma skin cancer.

Nanoparticles (AuNPs) are used for several different purposes within the biological field. For example, they are well suited for delivery of DNA into cells [19, 20], they can be used for vehicles for drug delivery and for killing tumorous cells [21, 22, 23, 24]. Recently they have gained interest as contrast enhancers in multiphoton laser scanning microscopy based on their multiphoton induced luminescence (MIL) [25]. The work presented in this thesis indicate that 10 nm monodispersed AuNPs is not detectable via MIL. Clusters of at least two AuNPs showed a MIL signal. This result is important to take into consideration when using AuNPs in biological tissues.

Chapter 2

Optical Microscopy and Spectroscopy

The word ”microscope” originates from the two Greek words for ”small” and ”to view” [26], which describe exactly what microscopy is: viewing something small. This is achieved by magnifying the object and increasing the resolution of the image. In optical microscopy, the object is exposed to light and the transmitted, reflected, or emitted signal is analysed. Spectroscopy gives information about the interaction between the light and the studied object. In fluorescence spectroscopy, the connection between excitation light and emitted light is studied [27]. This chapter gives a background to optical microscopy, and spectroscopy, along with a general introduction to fluorescence.

2.1 Optical Microscopy Fundamentals

The first optical microscope (containing two or more lenses) is generally considered to have been invented by father and son Hans and Zacharias Jansen of Middleburg, Holland around 1595. It consisted of two lenses and diaphragms mounted inside three sliding tubes, and possessed a magnification of three to nine times, which made objects like cells and bacteria visible. Even though the design of this microscope was simple, the microscopes used today are based upon the same principles [26].

The first reported optical microscopy experiments, in terms of examining objects and making drawings, are by Robert Hooke in 1665. He looked at a thin slice of cork and coined the expression ”cell” for the small sections he saw in the cork sample [26]. A decade later, van Leeuwenhoek observed several biological compounds, including bacteria, spermatozoa and red blood cells.

2.1.1 Restrictions to magnification and resolution

Magnification and resolution are the central features of microscopy. A high magnification makes it possible to study fine details but the field of view is narrow, and orientating in the sample can be difficult. Lower magnification gives less detailed information, but a larger field of view, which gives a better overview. Useful magnifications for studying biological tissues are in the range of 5 - 100 times, depending

on application. The resolution of an image is dependent on the entire setup, from the wavelength of the excitation light, to each individual optical compound in the beam path, such as lenses, mirrors, filters, and the objective.

The magnification and resolution are limited by aberrations and diffractions. The aberrations are effects occurring due to dispersion and the geometry of the lenses. The sample itself also contributes to aberrations. The aberrations can not be totally eliminated, but their effect on the final image can be minimized. Diffraction occurs when light is entering an aperture of the same size as its wavelength. This sets the final resolution limit, as the effect becomes dominant for higher magnifications. Although I have not worked specifically on investigating these effects, I will give a brief introduction to them, as they contribute to the final outcome of the image.

Aberrations can be classified as chromatic and monochromatic aberrations. Chromatic aberrations originate from dispersion, that is, from the fact that the refractive index is wavelength dependent. The blue colour will have the shortest focal length, green slightly longer and red the longest. If this is not corrected for, the image will show coloured fringes as in Figure 2.1. Monochromatic aberrations exist for any specific colour and refractive index. The dominating aberrations that determine the quality of the image are called the *Seidel aberrations: spherical aberration, coma, astigmatism, field curvature, and distortion* [28, 29, 30]. *Spherical aberration* has a strong radius dependence; rays entering the lens close to the rim contribute considerably more to the aberration than rays entering the centre of the lens. This aberration gives a blurry image as in Figure 2.1. *Coma* occurs when light is focused off the optical axis. The appearance of the image resembles a comet, and is visible when it comes to three dimensional imaging. *Astigmatism* gives rise to an image plane that has a concave shape in one plane along the optical axis and is linear in the plane perpendicular to the optical axis. *Field curvature* is similar to astigmatism, but the image plane is bent in both planes and the foci are created in a concave shape. The last Seidel aberration, *distortion* manifest as a tilted image plane.

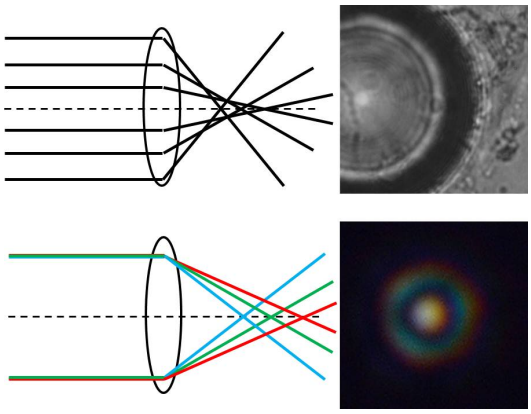

Figure 2.1: Top: Spherical aberration. Bottom: Chromatic aberration.

A common design for chromatic correction is to make the positive lens from crown glass, which has low dispersion, and the negative lens from flint glass, which has high dispersion. Combining these in a cemented doublet as shown in Figure 2.2a gives a correction for the red and blue light. Adding a third positive lens with low dispersion, an apochromatic lens is achieved, see Figure 2.2b, where the three wavelengths have the same focal point [28].

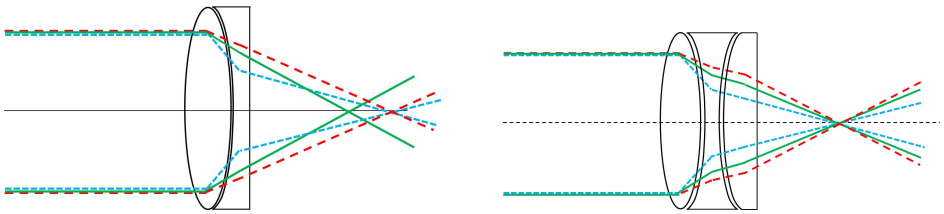

(a) Lens doublet. **(b)** Lens triplet.

Figure 2.2: Groupings of lenses for correcting chromatic aberrations.

The more advanced objective lenses for microscopy are designed to compensate for one or more aberrations; information of the intended corrections is given on the barrel of the objective. The nomenclature and abbreviations vary slightly depending on the manufacturer, but the following are some common terms: *Achro* or *Achromat* correct for axial chromatic aberration giving blue and red light the same focal point, while a higher order is *Apo*, or *Apochromatic* also correct for the green light. *Plan, Plano, Achroplan* give corrections for field curvature. Finally, *Corr, W/Corr, CR* denotes the presence of correction collar, by which the spherical aberrations can be corrected. Terms such as *Oil, Water, Glycerine* are also used, to specify the immersion type of the objective [31]. The reason for different types is to avoid refractive index mismatch. A water immersion apochromat objective was used in Papers I and II, and water immersion plan apochromat objective was used in paper III and IV. The choice for paper

I – III was based on the skin samples high containment of water. For paper IV it was chosen because the water gives higher numerical aperture than air, which is explained below.

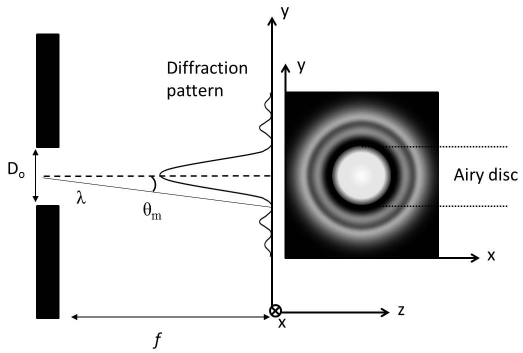

Figure 2.3: Diffraction originated from a circular opening with diameter D_o. The Airy disc is shown to the right

Diffraction effects occur when the aperture is of the same size range as the wavelength, see Figure 2.3, where the diffraction pattern is shown together with the Airy disc, which corresponds to the zeroth maxima. This sets a limit on the resolution, but cannot be corrected for in the same manner as aberrations. Choosing an objective with a high numerical aperture (NA), enables collecting more light and better resolution. The NA is defined as:

$$NA = n \cdot \sin\theta \tag{2.1}$$

where θ is the half-angle of the maximum illumination cone of the objective and n is the refractive index of the surrounding medium, see figure 2.4. Equation 2.1 shows the importance of the immersion media as it determines the amount of light that can be collected by the objective.

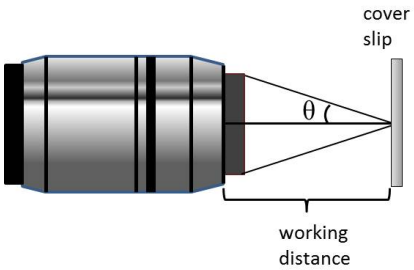

Figure 2.4: The working distance is measured from the front lens to the cover slip. θ determines the amount of light that can be collected.

As the resolution limit is in danger of being a subjective measurement, Lord Rayleigh's

criterion is often used as a standard. This says that the angle (θ_m) to the first diffraction minimum depends on the wavelength (λ) and the diameter D_o as

$$\sin\theta_m = 1.22\frac{\lambda}{D_o} \tag{2.2}$$

The closest distance between two objects should then be when the first diffraction minima for one of the objects coincides with the diffraction maxima of the other object, see Figure 2.5. Another resolution limit is given by Abbe's equation:

$$d = \frac{\lambda}{2NA} = \frac{\lambda}{2n\sin\theta} \tag{2.3}$$

where n is the refractive index of the surrounding medium. The resemblance between the two equations is obvious. Actually, equation 2.2 is valid as a resolution limit of a telescope, where the object is self-luminous. When Abbe scrutinized this relation and took into consideration the refractive index of the surrounding and that an object in a microscope is illuminated from outside, he came up with equation 2.3 [29].

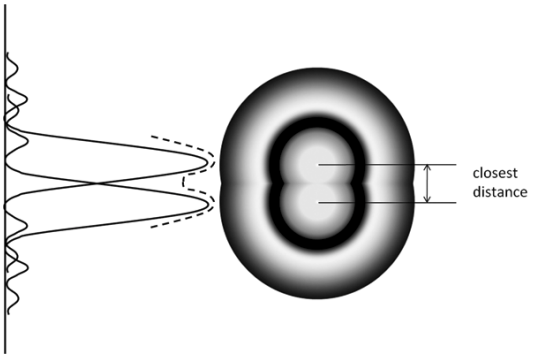

Figure 2.5: Two objects distinguished according to the Rayleigh criteria.

The working distance (wd) is also of importance as it gives an estimate of where the focus is found. The working distance is the distance from the nose lens of the objective to the top of the cover slip, see Figure 2.4. A long working distance is beneficial when working with thick samples, but then the NA becomes smaller. The choice between optimising wd and NA is a trade-off between the amount of light collected and the depth of the optical sectioning. Oil immersion objective lenses give higher NA, but if the sample has a high content of water (like many biological samples), there will be a mismatch in the refractive indexes.

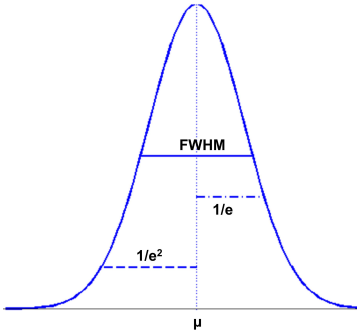

Figure 2.6: Gaussian curve.

Resolution can be measured by imaging sub-resolution beads, whose reflectance or fluorescent signal gives information about the resolution limit. The recorded intensity is analysed as full width at half maximum (FWHM), see Figure 2.6. The $1/e$ width is used for calculating the focal volume, and the $1/e^2$ width is used for calculating the diffusion coefficient [8, 32]. The Rayleigh criterion is the distance from μ to the minimum (the image show only one maximum).

2.1.2 The concept of fluorescence

Fluorophores are molecules that fluoresce when illuminated with light of a certain wavelength. Fluorescence is defined as the light emitted when a molecule is relaxing from an excitation level down to the ground level. The excitation process can be illustrated by a Jablonski diagram, see Figure 2.7, which shows the ground level, S_0 and the first energy level S_1. These states are singlet states (hence the notation S) which means the electrons in the shell have the spin configuration $+1/2$ and $-1/2$, giving a total spin of $S = 0$ [2]. The molecule in Figure 2.7 has absorbed a photon with energy $h\nu_{exc}$ and is excited to the second vibration level of S_1. It falls down to the zeroth vibration level of S_1 via a radiationless transition shown as a dotted crooked arrow [2]. The time the fluorophore spends in S_1 is called the fluorescence lifetime and is generally in the time range of ns [27].

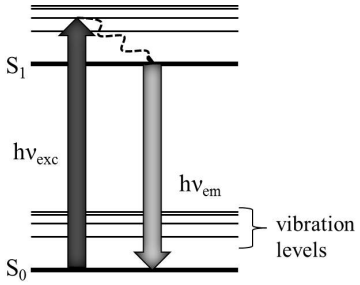

Figure 2.7: Jablonski diagram. The energy levels (thick lines) and vibration levels (thin lines) are shown.

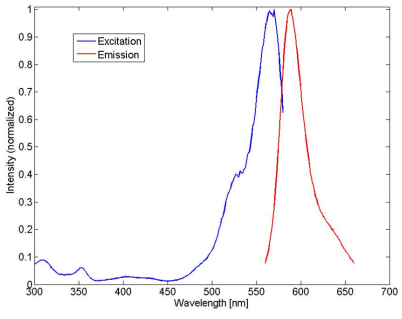

Figure 2.8: Excitation/Emission spectra for sulforhodamine B dissolved in water, demonstrating Stokes shift.

The wavelength difference between the absorption maxima and the emission maxima is called the Stokes shift. The spectra for Sulforhodamine B (SRB) in Figure 2.8 shows a narrow Stokes shift (around 10 nm) with a large overlap. If the absorption wavelength is longer than the emitted wavelength, the difference is called anti-Stokes. The emitted energy is then higher than the absorbed. This can occur if the molecule origins from one of the vibronic states of S_0 when excited. The probability of a populated vibration state is described by the Boltzmann distribution, and hence it is very small for a system at room temperature. However, it can not always be neglected, see Paper III.

Not all photons encountering the molecule will be absorbed. The probability of absorption is given as a cross-section $\sigma[cm^2]$ which can be seen as the effective area over which a single molecule absorbs the incoming light. The absorption probability can also be expressed as the molar extinction coefficient, ϵ which is defined as $\epsilon(\lambda) = N_a\sigma(\lambda)[cm^2mol^{-1}]$. If a molecule has absorbed a photon, there is a certain probability that this will result in an emitted photon. This probability is called the fluorescence quantum yield (Q) and is the ratio of the number of emitted photons to the number absorbed. Ideally Q is as close to unity as possible.

Fluorophores in a biological system can be categorised as intrinsic or extrinsic. The intrinsic fluorophores are those naturally inherent in the system and the extrinsic ones are added. Both intrinsic and extrinsic fluorophores can be used to enhance contrast in optical microscopy. Extrinsic fluorophores suitable for biological applications are numerous. A common fluorophore is the green fluorescent protein (GFP), which is naturally inherent in the luminescent jellyfish *Aequorea victoria*. The structure of GFP makes it fluoresce when it binds to a protein, which is useful for tracking proteins in both time and space [27, 33]. Probing DNA can be done by a large variety of fluorophores, for example ethidium bromide which has a naturally weak fluorescent signal is strongly enhanced upon binding to DNA. Another choice is 4',6-diamidino-2-phenolindole (DAPI), which shows a high signal when bound to the A-T nucleotides in the DNA. The families of fluoresceins and rhodamines, are used to track membranes and labelling of antibodies [27].

In Paper I, sulforhodamine B (SRB) was used as a model for the diffusion measurements. It was chosen because of its high solubility in water, its lack of pH-sensitivity and the significant difference between its emission peak and that of the autofluorescence. For Paper II, rhodamine B (RB) and rhodamine B isothiocyanate (RBITC) were chosen; the major reason for this was the unique property of RBITC, which is both reactive and an allergen. An additional reason which made it even more interesting for comparison purposes was the existence of previous work by Samuelsson *et al.* on fluorescein isothiocyanate, a close relative of this substance [34].

2.2 Laser scanning microscopy

In a widefield fluorescence microscope, the entire field of view is illuminated with the excitation light. This enables fast collection of data, but this is overshadowed by the main drawback which is poor axial resolution. Laser scanning microscopy (LSM) is generally equivalent to confocal laser scanning microscopy (CLSM), and provides high axial resolution. The resolution for a confocal setup is approximately 30% better than the resolution in a widefield setup [35]. In general, the confocal microscope is an epifluorescence setup, which means that the same objective is used for both excitation light and emitted light. The evolution in laser technology has made it possible to develop the CLSM technique into nonlinear laser scanning microscopy methods.

2.2.1 Confocal laser scanning microscopy

In CLSM, a laser beam is focused by a high-power objective, and then scanned across the sample; the emitted signal, coming from the focal volume is collected. The power of this method is the ability to move the focal point in the axial direction, enabling optical sectioning. There is no need to destroy the sample as with other techniques such as cryosectioning; it remains intact, and can be used several times. This also allows *in vivo* measurements in cells. The spatial resolution is controlled by a pinhole which excludes light coming from out of focus. The smaller the pinhole, the better resolution as more out of focus light is removed. Ideally, the pinhole should be infinitely small; which of course is not feasible. The smallest pinhole size depends on the application. Furthermore, the size of the pinhole will affect the intensity of the light reaching the detector. The larger the aperture, the higher the signal collected by the detector. Hence, there will be a trade-off between the resolution and the intensity. The emitted signal is collected in 'descanned' mode, and is scanned to the detector by the scanning mirrors.

The resolution in CLSM is measured by using subresolution beads as described in Section 2.1.1. A three- dimensional image of the bead is obtained by sectional scanning, giving information about the resolution in both the lateral and axial direction. The resolution is worse in the axial direction than in the lateral, see Figure 2.9. The image of the bead is elongated in the axial direction, which is a diffraction effect. The bent shape is due to the aberration coma, see Section 2.1.1. The intensity profile from the beads gives a measurement of the resolution. Figure 2.10 shows the lateral resolution of three different constellations of beads with corresponding intensity profiles.

2.2.2 Nonlinear optical microscopy

The optical laser scanning microscopy techniques described above are not the only such techniques in existence; another type comprises those based on nonlinear optical processes. The term 'nonlinear' originates from the relation between a dielectric material and incoming light. When the material is considered at an atomic level, the molecules can be seen as oscillating dipoles, which will change their oscillating frequency when irradiated. For a fluorescent material, the irradiation gives rise to an emitted signal, which depends linearly on the irradiation. This can be expressed in

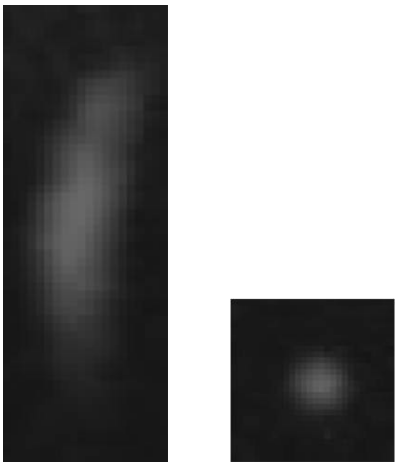

(a) Aberration and diffraction in the axial plane.

(b) Diffraction in the lateral plane.

Figure 2.9: Aberrations and diffraction in microscopy. The object is a fluorescent bead of 175 nm.

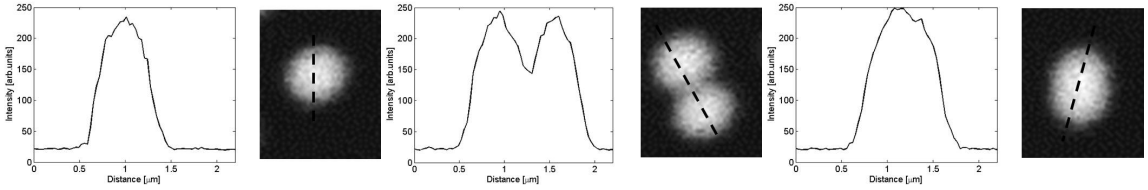

(a) Single bead **(b)** Two beads **(c)** Two unresolved beads

Figure 2.10: Intensity profiles for three bead constellations.

terms of the polarization $\mathbf{P}$ of the material and the electric field $\mathbf{E}$ of the incoming light:

$$\mathbf{P}(t) = \chi^{(1)}\epsilon_0\mathbf{E}(t) \tag{2.4}$$

where ϵ_0 is the permittivity, and $\chi^{(1)}$ is the linear, electric susceptibility [2, 36, 37]. The susceptibility is dimensionless, and can be explained as the collective displacement of the charges in the material. Equation 2.4 above is linear, as long as the field strength $\mathbf{E}$ is moderate. If the field strength becomes too high, the oscillating charges will reach a saturated level; their response can be expressed as a power series expansion:

$$\mathbf{P}(t) = \epsilon_0 \left[\chi^{(1)}\mathbf{E}(t) + \chi^{(2)}\mathbf{E}^2(t) + \chi^{(3)}\mathbf{E}^3(t) + \ldots\right] \tag{2.5}$$

where $\chi^{(2)}$ is the second-order susceptibility, $\chi^{(3)}$ is the third-order susceptibility, and so on. The linear susceptibility is much larger than the nonlinear terms, which is the reason for the high intensities needed for nonlinear optical processes.

One nonlinear method suited for biological samples makes use of a non-linear scattering process konown as second harmonic generation (SHG). SHG, which was first observed in 1961 by Franken [38, 39], is based on an interaction between two photons of equal energy which produces a third photon of exactly twice the energy, i.e. half the wavelength, of the incoming light. It can be used as a contrast mechanism in optical microscopy, and was first used to investigate aluminium and gold surfaces. In the biological field, it has been used for probing membrane potentials and imaging of biological tissues. The collagen and elastin of excised human skin respond to SHG with an excitation wavelength of 800-840 nm [40, 41, 42]. The combination of SHG and the method of two-photon excitation laser scanning microscopy (which is introduced in the next section) can be used for tracking changes in collagen formation in the dermis. One of the advantages of this is that the same excitation wavelength can be used for both and so, only one illuminating source is required. In addition, the emitted signals differ significantly and can be separated to different detectors. The drawback of SHG is that the collected signal can be weak and high input intensity is needed. It is not possible to distinguish different chemicals, using SHG as a single tool.

Coherent anti-Stokes raman scattering (CARS) spectroscopy is another nonlinear method commonly used within the biological field. This technique is based on the intrinsic vibrational spectra of the molecules which makes it possible to distinguish specific molecules [43, 44, 45]. Three photons interact with the molecules and generate a forth photon, an anti-Stokes photon [46]. Two photons are used to transfer the molecule to a vibrational state and a third photon of frequency ω_p is anti-Stokes scattered, resulting in a generated CARS photon of frequency $\omega_{CARS} = 2\omega_p - \omega_s$. For excitation, the frequency difference $\omega_p - \omega_s$ is tuned to match a molecular vibrational resonance frequency (ω_{vib}), that is, $\omega_p - \omega_s = \omega_{vib}$.

The focus of my work is the technique of two-photon laser scanning microscopy (TPLSM), which has been given a section of its own.

2.3 Two photon microscopy

In CLSM, one photon interacts with the fluorophore for electronic excitation, while in TPLSM, the energies from two photons are needed to excite the molecule. The possibility for two photons to be simultaneously absorbed is much lower than for one photon absorption, so the two-photon excitation process will only occur in the focal spot where the intensity is sufficiently high.

Using two photons instead of one pushes the penetration limit for biological tissue. In optically turbid media the resolution is significantly better for two photons than for one, see for example reference [47] where CLSM and TPLSM performed on different biological samples are compared. Theoretically though, the resolution in CLSM is better than that in TPLSM, due to Abbe's equation (see equation 2.3), as shorter wavelengths are used for confocal microscopy. In reality, the resolution becomes similar for the two methods, due to the elongated focal region of confocal microscopy which

causes mixing of the signal from different layers and blurring of the image.

2.3.1 Two-photon excitation, TPE

The two-photon excitation (TPE) can be illustrated by the Jablonski diagram, see figure 2.11. Apart from the excitation energy, that is constituted of two photons, the event is similar to the one photon excitation in figure 2.7. The molecule is assumed to be found in the ground state S_0. The absorption of two photons within a time interval of 10^{-16} seconds excites the molecule to the first electronic state S_1. The wavelength should be approximately twice of that for one-photon excitation.

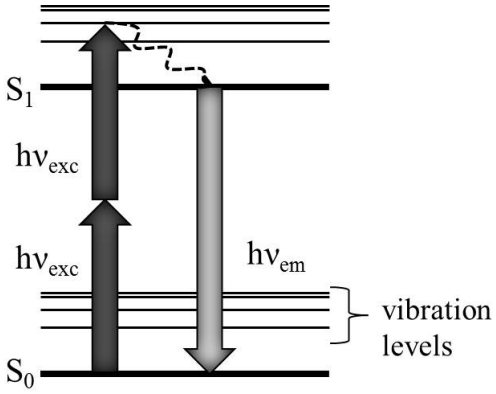

Figure 2.11: Jablonski diagram for TPE.

2.3.2 Lasers

Non-linear microscopy requires a high intensity laser, but the risk of damaging the sample must be taken into consideration. A conventional continuous wave laser is not a good choice, as it carries too high a risk of damage. The solution is to use a pulsed laser, where the beam is not continuous but consists of a train of pulses; see Figure 2.12. The advantage of this technique is although each individual pulse has a high power (of the range of kW – MW), the average power is only moderate (in the range of mW – W). The laser is either Q-switched, which is used for nanosecond lasers, or mode-locked for femtosecond lasers [48]. The idea behind the Q-switched lasers is to block the feedback of light in the cavity. The excitation is then built up in the medium which give a high accumulated energy. When the Q-switch opens, a pulse with high power is produced. The time the Q-switch is closed determines the repetition rate of the laser, which is typically between 1 and 100 kHz. The produced pulses are normally in the nanosecond range, and can have very high peak power, around megawatt. A common medium used in ns lasers is neodymium-doped yttrium aluminum garnet (Nd:YAG).

Common lasing media for mode-locked lasers include ion-doped crystals and glasses. One of the most popular choices is the Ti:Al_2:O_3-laser, more commonly known as the Ti:Sapphire-laser. The principle behind the mode-locking technique is to block parts of the beam with an advanced shutter, such as an acousto-optic modulator (AOM), shown in Figure 2.13. The frequency of the pulse train depends on the cavity length, L, and the velocity of light, c, as shown in Figure 2.12. The frequency of the femtosecond Ti:sapphire-laser used in Papers I and II is 83 MHz, which corresponds to a cavity of 1.8 m. Figure 2.13 shows how this inconveniently large size can be avoided. The cavity is folded by mirrors M_4 and M_5 and focused by mirrors M_2 and M_3. Mirrors M_6 to M_9 direct the beam through the prisms P_1 to P_4, thus compensating for cavity dispersion. The slit between P_2 and P_3 is used for selecting wavelength, via the tuning slit position control in Figure 2.14. Normally, the prism dispersion compensating control must also be adjusted when changing the wavelength. The mode-locking element, the (AOM), consists of a transparent crystal (commonly used is quartz), which is equipped with a radio frequency driven piezoelectric transducer. This generates a diffraction grating within the crystal. Matching the modulation frequency to $c/2L$ give the laser repetition rate. Here, the cavity length is adjusted to give the correct frequency. The output signal is divided in the beam splitter, where a part is sent to the AOM driver which sends a signal to the AOM.

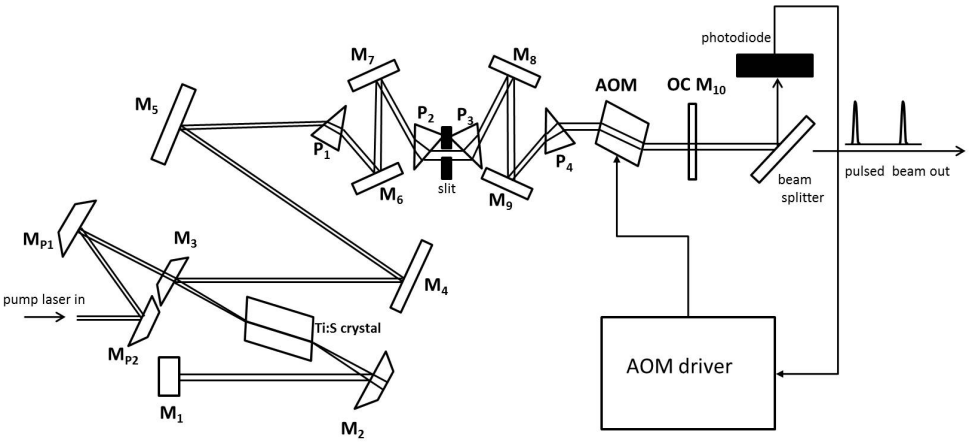

Figure 2.13: Simplifyed beam path inside a mode-locked laser. The cavity length L is the distance from M_2 to M_{10}

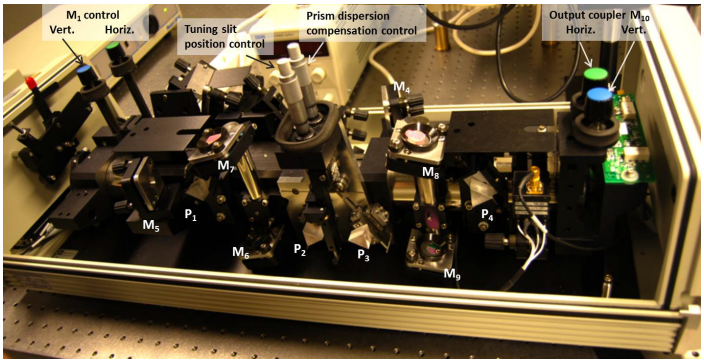

Figure 2.14: The Ti:sapphire Tsunami laser in our lab, without the protecting shield

For a wavelength of 800 nm, and a pulse with an FWHM of 50 fs, the calculated smallest FHWM for the bandwidth gets around 3.4 nm for NIR light due to the Heisenberg uncertainty principle[1] [37]. This gives a rather large difference of the maximum and minimum wavelength that fits within a pulse. Due to dispersion in the optics, the pulse arriving at the microscope will be much wider. This is called group velocity dispersion (GVD) and is said to have a positive 'chirp' if the red wavelengths goes faster than the blue. This can be corrected for by introducing prism pairs which create the opposite chirp to narrow the bandwidth of the pulse. In a Ti:sapphire

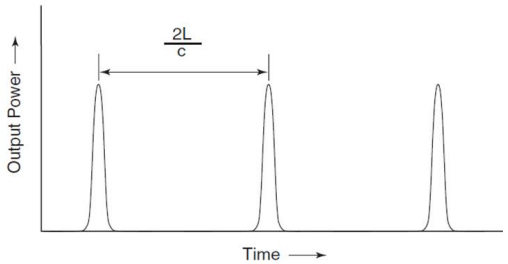

Figure 2.12: The pulse train.

[1] $\Delta E \Delta t \geq \hbar/2$

laser, the titanium doped sapphire crystal introduces a positive chirp to the pulse, which is corrected for by the prism pair P_2 and P_3 in Figure 2.13 and Figure 2.15.

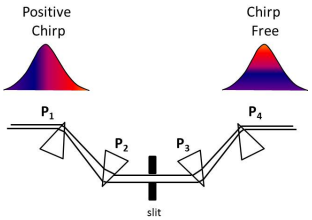

Figure 2.15: Prism P_2 and P_3 introduces a negative chirp.

It is standard procedure to realign the laser beam very time it is switched on. Figure 2.16 show the lasers during a thorough alignment of the pump laser to the Ti:sapphire laser.

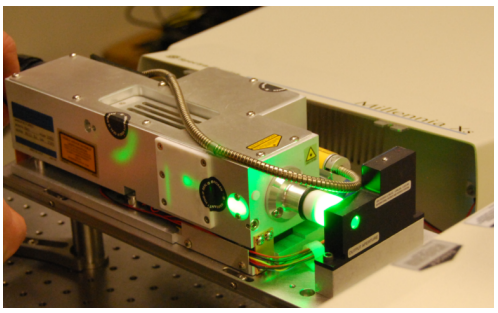

(a) The pump laser, MillenniaX.

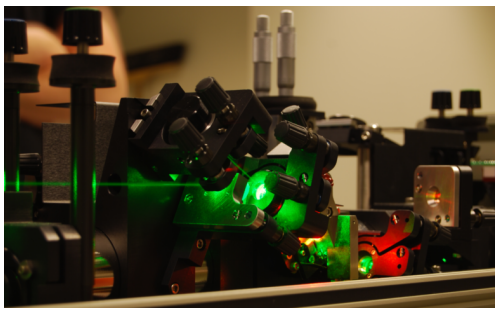

(b) The mode-locked Ti:sapphire laser. The green laser beam is from the pump laser.

Figure 2.16: Alignment of lasers for TPLSM setup.

2.4 Fluorescence Correlation Spectroscopy

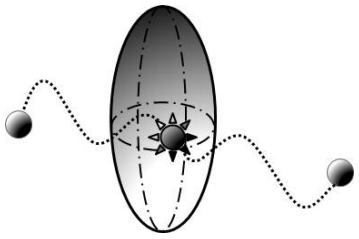

Figure 2.17: Three dimensional diffusion of a molecule.

Fluorescence correlation spectroscopy (FCS) is a sensitive method used for high resolution analysis of molecular diffusion. It allows the user to measure low molecular concentrations (in the range nanomolar to micromolar) randomly moving in and out of a small excitation volume [32]. The principle is to measure the fluorescence signal as a function of time and then analyse it by autocorrelation. The signal is recorded via single photon counting with a sensitive photon counter, such as a photomultiplier tube (PMT), an avalanche photo diode (APD) or a charge-coupled device (CCD) camera. The first reported attempt at FCS was in 1972, by Magde *et al.* [49], who measured the diffusion and binding of ethidium bromide to DNA. Since then, the technique has been widely used in several different disciplines, for applications such as measuring diffusion in solutions [50], measuring diffusion in membranes [51] and measuring molecular aggregation [52, 53]. Other applications of FCS include molecular dynamics in cells, which has been reported by for example Schwille *et al.* [54, 55]. FCS and TPLSM have been used in combination on living cells by Berland *et al.*; and Wang *et al.* [56, 57]. Alexandrakis *et al.* reported two-photon excitation laser scanning microscopy fluorescence correlation spectroscopy (TPFCS) measurements in tumor tissue in 2004 [58]. The most recent reports within the biological field includes studies of protein transports [59], interactions between fluorophores and DNA nucleotides [60], bioconjugation of quantum dots and cellular uptake of quantum dots [61, 62].

Diffusion is a huge area within biomedical studies, and this thesis is concerned with only a small fraction of the field. Papers I and II, investigate molecular diffusion within human skin. These papers are to the best of my knowledge the first reports of TPFCS in human skin. In the long term, one possible application of this work is to understand the processes and interactions of topical drug delivery and allergen-protein forming. Diffusion plays a major role in this context, and so it is important to develop a trustworthy method for these measurements.

2.4.1 Diffusion Theory

Diffusion is a form of transportation that is relevant to a wide range of disciplines, from solid state physics (travel of single atoms within a lattice) to molecular motion in biological tissue [63]. The concept of diffusion includes both totally random movement, and movement due to inhomogeneities, i.e. concentration differences. The relation between the diffusion flux and a concentration gradient is often expressed in Fick's first law [37, 63]:

$$J = -D\triangle C \tag{2.6}$$

where J (mol /m^2s) is the flux of molecules, D (m^2/s) is the diffusion coefficient and C (mol/m^3) is the concentration of particles. The minus sign indicates that the flux is

directed along the negative concentration gradient; that is, from high concentration to low. The equation is still valid even if the flux is zero. However, the true driving force of the diffusion, is not the concentration gradient, but rather the chemical potential μ.

$$J = -\kappa \triangle \mu \tag{2.7}$$

$$\mu = -T \left(\frac{\partial S}{\partial N} \right)_{E,V} \tag{2.8}$$

where T is the temperature, S is the entropy and N is the number of particles. For a system at constant pressure and temperature, the relation between the thermodynamic transport coefficient κ and D is expressed as $\kappa = DC/RT$, where R is the molar gas constant [64, 65]. In Papers I and II, D is obtained from the TPFCS measurements. The Stokes-Einstein equation is used to estimate the hydrodynamic radius, R_h, of the diffusive molecules [32, 54, 66]:

$$D = \frac{k \cdot T}{6\pi\eta R_h} \tag{2.9}$$

where k is Boltzmann's constant, T is the temperature and η is the viscosity of the medium.

Free diffusion occurs for molecules evenly distributed in a homogenous medium. If there are heterogeneities, or the molecules are interacting with compounds in the medium, it is called anomalous diffusion. If there is a concentration gradient of the molecules in the medium, the movement will occur along the gradient to even out the differences. If the molecules bind to a compound that has a velocity, the movement is not diffusion but active transportation. Diffusion can occur in two dimensions, if there are restrictions in the surroundings, for example diffusion within a membrane. Three dimensional diffusion occurs for example within the cytoplasm of a cell [32]

2.4.2 Measuring and analysing FCS

In this thesis, FCS has been used for investigating the diffusivity, size and accumulation of the molecules based on a methodology described by Schwille *et al.* [32].

The correlation function is based on denoting the intensity at a certain time t to $F(t)$ and express the fluctuations around a mean value as:

$$\delta F(t) = F(t) - \langle F(t) \rangle \tag{2.10}$$

where $\langle F(t) \rangle$ is the time average of the fluorescence intensity. The normalized autocorrelation function is given as:

$$G(\tau) = \frac{\langle \delta F(t) \cdot \delta F(t+\tau) \rangle}{\langle F(t) \rangle^2} \tag{2.11}$$

In this equation, the intensity at time t is compared with the intensity at the time t + τ, where τ is the lag time and is usually in the range of 10^{-2} to 10^{2} ms [27, 32]. Further information about the diffusion is achieved from the free three-dimensional

autocorrelation fit [32]:

$$G(\tau) = \frac{1}{V_{eff}\langle C\rangle} \cdot \frac{1}{1+\frac{\tau}{\tau_d}} \cdot \frac{1}{\sqrt{1+\left(\frac{r_0}{z_0}\right)^2 \cdot \frac{\tau}{\tau_d}}} \tag{2.12}$$

where r_0 and z_0 are the lateral and axial radii of the focal volume and τ_D, the diffusion time, is the mean time the molecule stays in this volume. This equation can be deviated from equation 2.11, by several assumptions and approximations [32]. A collected fluorescence signal from a randomly moving molecule, and corresponding autocorrelation curve are shown in figure 2.18. The autocorrelation fit was obtained by fitting equation 2.12 to the autocorrelated data in MatLab by using a Levenberg-Marquardt algorithm. The number of molecules in the focal volume (N) and τ_D are information

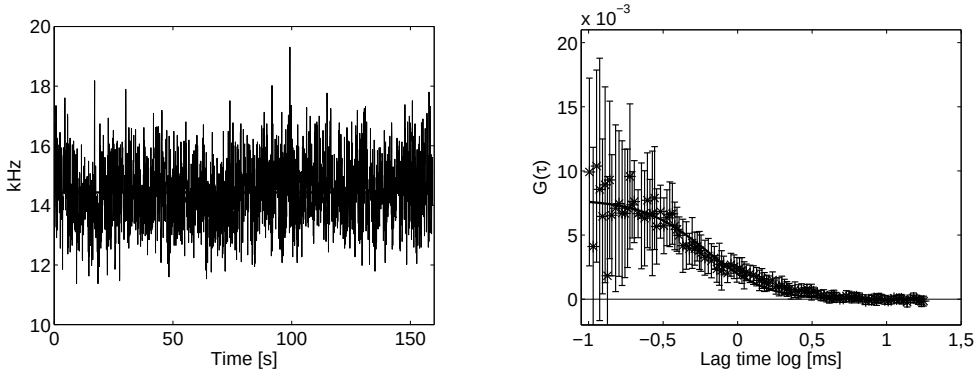

(a) Fluorescence signal recorded during 160 seconds.

(b) Autocorrelation curve with free 3D fit (black solid line).

Figure 2.18: Fluorescence correlation spectroscopy.

that is achieved direct from the autocorrelation. When $\tau \Rightarrow 0$, the autocorrelation function $G(\tau)$ corresponds to $1/V_{eff}\langle C\rangle$, see equation 2.11. The value of $V_{eff}\langle C\rangle$ corresponds to the average number of molecules in the focal volume. The diffusion time is given as the lag time for half of the amplitude of $G(\tau)$ [32, 66]. Examples of other sorts of correlation fits are for two dimensional membrane diffusion:

$$G(\tau) = \frac{1}{V_{eff}\langle C\rangle} \cdot \frac{1}{1+\frac{\tau}{\tau_d}} \tag{2.13}$$

and for active transport:

$$G(\tau) = \frac{1}{V_{eff}\langle C\rangle} \cdot \frac{1}{exp(-(\tau \cdot \nu / r_0))} \tag{2.14}$$

FCS can be measured with a confocal, or two-photon, microscopy setup. For multispot imaging, a bundle of optical fibers can be used, each one connected to a PMT or CCD [67, 68]. An acquisition card which can collect the data with high time resolution, and perform the correlation analysis is also needed.

Equation 2.12 was used in Papers I and II for the analysing the quantitative measurements in skin. The parameters r_0 and z_0 were obtained from the PSF measurements.

Other related methods for quantitative measurements in biological tissues are time-correlated single-photon counting (TCSPC) and fluorescent lifetime imaging microscopy (FLIM) [69]. TCSPC is built upon counting the photons emitted after the excitation pulse, building up a histogram. The trend of the histogram gives the fluorescence decay profile, which tells the lifetime of the fluorophore, i.e. how long it remains in the excited state after excitation [27]. This time is normally in the 10 ns size. The diffusion and lifetime τ is related as: $\delta x^2 = 2D\tau$, where δx is the average diffusion length. The relation is mostly used for determining δx out of D and τ. FLIM is related to TCSPC, as it relays on the lifetimes of the present fluorphores. The emitted intensity dependence of the lifetime can be used for creating an image of a sample as different fluorophores have different lifetimes. It gives information and identification possibilities about the specific fluorophores and their localization [27, 69].

Chapter 3

Biomedical Studies

The techniques and methods described in Chapter 2 have been used on human skin to gain knowledge about diffusion and accumulation of molecules, and for tumour detection. They have also been used on gold nanoparticles (AuNPs) in order to investigate their multiphoton induced luminescence (MIL) properties.

This chapter will give an introduction to human skin in terms of structure, optical properties and suitable microscopy techniques. It will also give a background to the AuNPs, where the theory behind the one and two photon excitation of AuNPs is described and the synthesis and biological applications are discussed.

3.1 Human Skin

Skin is the largest of our organs and also the most exposed; as a consequence, it is subjected to foreign compounds and electromagnetic radiation on a daily basis [70]. Common skin-related problems include contact allergy and cancer. Contact allergy is not lethal, but will cause the patient pain and discomfort [71]. Common skin cancers are the non-melanoma family, which do not metastasize, but can cause severe destruction of the skin tissue leading to loss of function and deformation [72].

Contact allergy is caused by molecules called haptens. The allergic reaction is triggered when the haptens bind to proteins in the skin, forming hapten-protein complexes. The formation is believed to take place in the epidermis, but it is not fully understood exactly where; this is important to investigate further [71]. Non-melanoma skin cancer can be successfully treated by photodynamic therapy (PDT) in a method based on the fluorophore protoporphyrin IX (PpIX) [73]. PpIX occurs naturally in skin, but for PDT the production is locally enhanced by topical application of aminolevulinic acid (ALA), or methylaminolevulinate (MAL).

3.1.1 Structure and functions

The skin consists of three main layers: the subcutis, dermis and epidermis [70]. The bottom layer, the subcutis, consists of adipose tissue (fat) and areolar connective tissue (fibres). The next layer, the dermis, is composed of connective tissue containing collagen and elastic fibres. This combination makes the skin extensible and elastic. The top layer is called the epidermis and is composed of keratinized stratified squamous epithelium, see Figure 3.1. The epidermis is usually divided into four sublayers. In the border between the dermis and epidermis is the stratum basale, where the cells multiply and are pushed upwards to the higher layers. The next layer is called the stratum spinosum and consists of about ten layers of keratinocytes. After this, comes the stratum granulosum (SG), which consists of five layers of flattened cells growing in a honeycombed pattern. Finally, the top layer, is the stratum corneum (SC), which is around 15 - 20 μm thick and contains of about 30 layers of flat dead keratinocytes that lack nuclei [74].

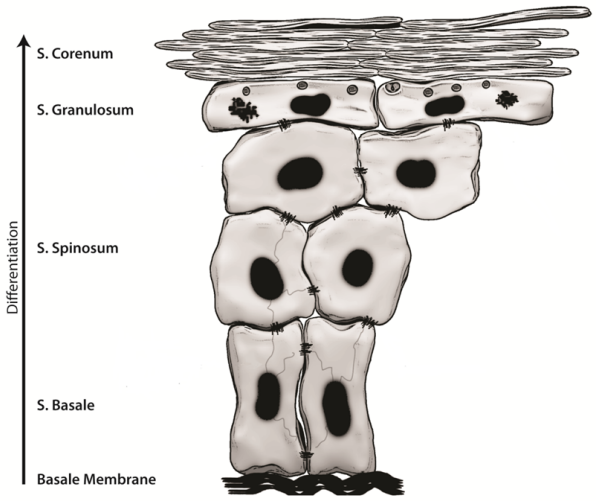

Figure 3.1: A schematic illustration of the skin layers in epidermis.
Image used with permission from Carl Simonsson

This characterization of the cells and the different skin layers is true for healthy skin. For skin disorders such as non-melanoma cancer, the cells can show abnormal shape, and are disorganised among the layers, which can be visualised using TPLSM [11, 15].

3.1.2 Optical properties of skin

Biological tissue in general possesses high scattering and absorption coefficients for visible light, which makes optical microscopy difficult [75, 76]. A scattering photon can go in any direction, and can be scattered multiple times before being absorbed or transmitted. The optical properties of skin are determined by several autofluorescent compounds see Table 3.1.
Both scattering and absorption are wavelength dependent, and the components water,

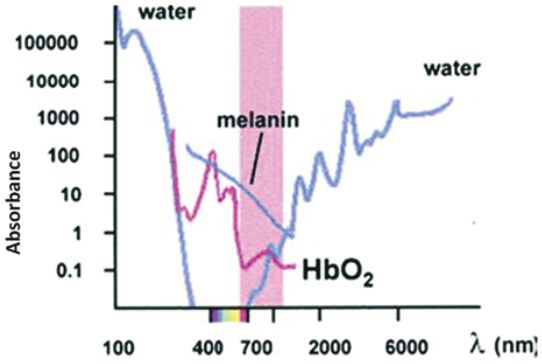

Figure 3.2: The absorption-wavelength dependence for the main absorbing compounds in the intracellular environment. Modified from [9].

melanin and hemoglobin have low absorption coefficients for wavelengths between 600 and 1100 nm, see Figure 3.2 [9]. This spectral range is called "the optical window" as the skin is literally an open window here. The scattering properties of skin are also wavelength dependent, but the variations are smaller than for the absorption properties. The scattering decreases from 250 to 1500 nm [75].

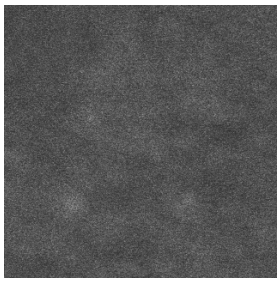

(a) Signal from the autofluorescence

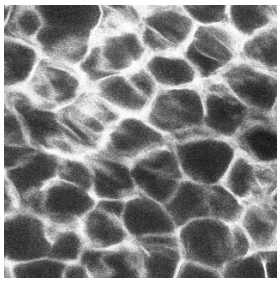

(b) Signal from sulforhodamine B

Figure 3.3: Human skin at a depth of 10 μm from the surface. Field of view is 200 x 200 μm.

Extrinsic fluorophores can be added to the skin for imaging. It is important that the emission spectrum of the added fluorophore differs from that of the autofluorescence. The images in Figure 3.3 show the same skin sample viewed under different filter settings to image either the autofluorescence in 3.3a or the fluorophore, which in this example is sulforhodamine B 3.3b. The skin in general correlate well with TPLSM, there are several references that reports good results. The collagen can be imaged with SHG, which together with TPLSM provides an interesting contrast mechanism [40].

Table 3.1: Data over common fluorophores in skin

Component	Skin layer	Exc/Em wavelength [nm]	Method
NAD(P)H	SG [11]	340/(450 – 470) [11, 27]	TPM [77]
keratin	SC [75, 78]	485 [79] /525 [80]	TPM [80]
melanin	SB [11]	UV – visible/(440, 520, 575) [11]	TPM [81]
elastin	Dermis[11, 82]	(300 – 340)/(420 – 460) [11]	TPM [83], SHG [2]
collagen	Dermis [11, 82]	(300 – 340)/(420 – 460) [11]	TPM [83] SHG [42, 40, 2]

3.1.3 TPLSM in human skin

The first report of TPLSMM on human skin appeared in 1997, when Masters *et al.* examined the autofluorescence of human skin *in vivo* [10]. This pioneering work was followed by several reports, the majority of which dealt with the investigation of autofluorescence for distinguishing healthy skin from diseased skin. For example, the use of excitation scans to examine autofluorescence of *in vivo* skin was reported in 2010 by Breunig *et al.* [84]. Later, in 2012, Yu *et al.* reported similar investigation extended to also cover the emission spectra [79]. The authors mapped out the spectra from inherent fluorophores for healthy skin and diseased skin; a technique which could in the future be used as a diagnostic tool. SHG and TPM were used in combination by König *et al.* in 2003 to detect collagen, comparing healthy skin with disordered skin [11].

Allergic contact dermatitis is a common disease. It is caused by haptens that bind to proteins in the skin, forming hapten-protein complexes that then trigger the allergic reaction. The formation of these complexes is believed to take place in the epidermis, but it is not fully understood exactly where [85]. Paper II investigates the dynamics of these hapten-protein complexes, motivated by previous work by Samuelsson *et al.* [34].

Other more severe skin-related diseases include non-melanoma skin cancer. These tumours do not metastasize, but can cause severe destruction of the skin tissue, leading to loss of function and deformation [72]. One treatment that has been successful in this, area is PDT [73]. This method is based on the fluorophore protoporphyrin IX (PpIX) which occurs naturally in skin, but for PDT, the production is locally enhanced by topical application of aminolevulinic acid (ALA). The first report on clinical use is from 1990 by Kennedy *et al.* who reported a promising outcome [86]. The accumulation of PpIX in tumor cells has been found to also work as a diagnostic tool [87, 73].

3.2 Gold nanoparticles (AuNPs)

There are several reasons for investigating AuNPs in biological tissues. Due to their size and versatility, they can be used for delivery of molecules into cells, drug delivery

and for detecting, imaging and killing tumor cells [19]. As those applications mean examining the sample in a microscope, preferably a TPLSM, it is of high importance to understand their luminescence properties.

3.2.1 Optical properties

The optical properties of AuNPs are very different from those of gold in bulk state. A piece of gold in bulk state is yellow in colour, while a solution containing AuNP can show a wide range of colors, from pale pink to a deep green [88]. The colour of the AuNP solution depends on parameters such as the size, shape and symmetry of the nanoparticles. For spheres, the colour goes from pale pink to deep red with increasing diameter, see Figure 3.4. For rods, the color depends on the ratio of the long and the short axis and goes from pale pink to brown, via blue and green. The colour changes of the rods are more dramatic than those of the spheres, which all lies in the red wavelength area.

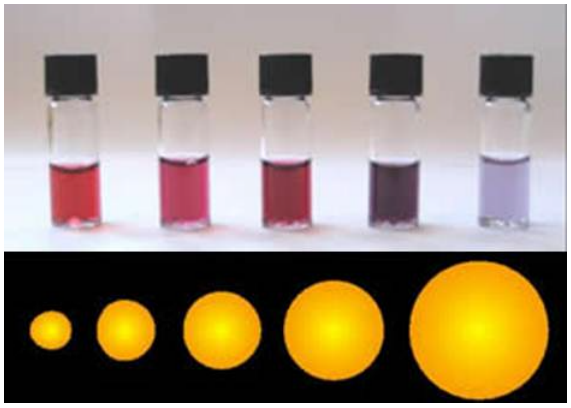

Figure 3.4: Diameter-color dependence for solutions of AuNPs. Figure is used with permission from the website webexhibits [89].

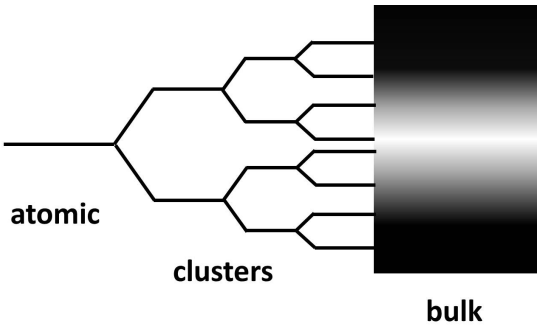

Figure 3.5: Energy levels going into band structure. Modified from [90, 91].

For a single atom, each electron occupies a specific quantum state. For clusters of atoms, these energy levels become more and more complex although they are still separated. For bulk systems, the energy levels become so close that they merge into continuous energy bands, see figure 3.5. The outermost of these bands is called the conduction band; the electrons within this band do not belong to a specific atom, but to the collective of atoms. The next layer is the valence band, with electrons bound to single atoms. Between the conduction band and the valence band is an energy gap that determines the conductivity of the material [90, 91].

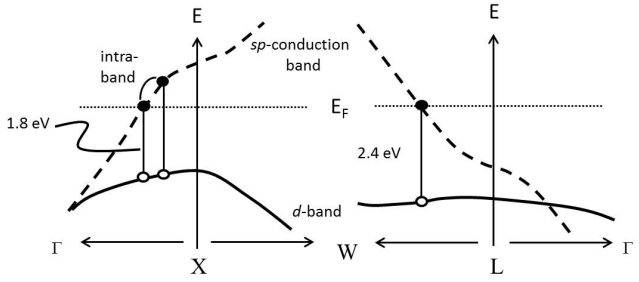

Figure 3.6: Electron-hole pairing between the d and sp bands. Modified from [92, 93]

The valence band for gold is constituted of the electrons in the $5d^{10}$ orbital, and the conduction band is constituted of the electrons in the $6s^1$ band which is the highest occupied energy level. The non-occupied levels that follow also belongs to the conduction band; the first of these is the 6p band [94]. For gold in bulk state, the energy levels are merged into each other, and the gap is considered nonexistent, bulk gold is a good conductor. Gold clusters in the nanoscale exhibit an energy gap, for which the width is dependent on the size of the nanoparticle. For AuNPs of diameters in the range 10 – 20 nm, the gap is around 2.4 eV, which gives an absorption spectra with a sharp peak around 520 nm [20, 91]. This gap is shown to the right in figure 3.6. For particles smaller than 2 nm, the absorption spectra is flattened out and does not show the distinct peak at 520 nm. Instead the spectra show an onset around 1.6 –1.8

eV, which corresponds to intraband transitions, shown to the left in figure 3.6 [92, 95]. The intraband transistions corresponds to electron-hole pairing within the conduction band. Radiating the particles with a wavelength with an energy corresponding to the energy gaps will cause a resonance effect known as the surface plasmon resonance [90, 96].

Excitation due to absorption of more than one photon is a different process for a nanoparticle than a molecule. The correct term is multiphoton induced luminescence (MIL) to distinguish the process from fluorescence, where the photons are absorbed simultaneously. MIL is originated from a sequential absorption of two photons. The first photon excites an electron in the *sp* conduction band below the Fermi surface. This electron reaches the *sp* conduction band above the Fermi surface by absorbing a phonon (crooked line in Figure 3.7). This corresponds to an intraband transition as it occurs within the conduction band. This process gives a hole available in the *sp* band below the Fermi surface, and the second photon can excite an electron in the *d* band up to the *sp* band [63, 97].

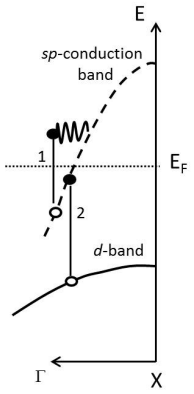

Figure 3.7: Sequential one-photon absorption. Modified from [97]

3.2.2 Synthesis

Two of the most commonly used methods to prepare AuNPs are the Turkevich method developed in 1951, and the Brust method developed in 1994 [98, 99]. The Turkevich method is based on chloroauric acid ($HAuCl_4$) which is reduced by adding sodium citrate. The size of the particles that Turkevich obtained with this method was 20 nm, with variations depending on the amount of added sodium citrate. The possible size distribution was later fine-tuned by Frens *et al.* who worked with small changes of the ratio between the ($HAuCl_4$) and the sodium citrate [20, 100, 101]. The Brust method provides smaller particles, between 1 – 3 nm. The synthesis is described as a water-toulene reduction of $AuCl_4$ by sodium borohydride in the presence of an alkanethiol [20, 99]. This method gives AuNPs with higher thermal and air stability than the Turkevich method.

AuNPs can be deposited on different surfaces by e.g. the spin coating technique. This gives a surface with evenly distributed particles [102]. The particles can also be deposited on a surface by electrodeposition [103].

3.2.3 Biomedical Applications

The AuNPs can be used for delivery of DNA into cells, as 'gene guns', where the DNA is adsorbed onto the surface of the AuNP, and then shot into the cell. This is an effective method of introducing DNA into cells with rigid cell walls. Another method of transferring molecules into cells is via engulfing the AuNP-molecule complex by the cell [19].

There are several reports where AuNPs have been used for detecting and killing tumor cells [104, 105]. Durr *et al.* reported on rod-shaped AuNPs that enchance the MIL signal for imaging of cancer cells [106]. Recently, Balla *et al.* report of less heating of nanorods when exciting a wavelength different from the absorption maximum [107]. Application of AuNPs on skin have been reported by Labouta *et al.* who report on measurements of PSF at a depth of 14 μm in skin [108].

The size of the AuNPs are of high importance, as this is one of the crucial factors for their penetration ability, whether the target is a cell or tissue. Unfortunately they have a tendency to form clusters, even in the presence of a reducing agent such as sodium citrate [98, 100, 101]. This is the seed for the investigation in paper IV.

Chapter 4

Methods

This chapter presents the methods used within my work and describes the skin preparation along with the fluorophores and nanoparticles.

4.1 Skin preparation

Experiments were performed on excised healthy skin in Papers I and II. The samples were frozen in -70° C and thawed before use. Fresh tumour samples were used in Paper III, examined within an hour after surgery. A healthy sample from the same patient was used as a control.

4.1.1 Excised skin preparations for diffusion experiments

The diffusion experiments in paper I and II were performed on excised healthy skin. It was obtained from breast reduction surgeries at Sahlgrenska University Hospital in Gothenburg, Sweden. The samples were collected after surgery, cut into 1 x 1 cm pieces, and stored at -70° C for 1 - 10 months. Special laboratory equipment is required when preparing skin for investigation of its physical properties. The glass diffusion cell shown in Figure 4.1 was developed for transdermal drug delivery research [109]. The skin sample is placed on top of the glass cell so the surface is exposed to the solution in the donor compartment. The metallic clamp keeps the skin in place and prevents the donor solution from leaking. Samples can be extracted from the acceptor compartment without affecting on the diffusion process. Constant temperature is ensured by circulation fluid and a magnetic flea.

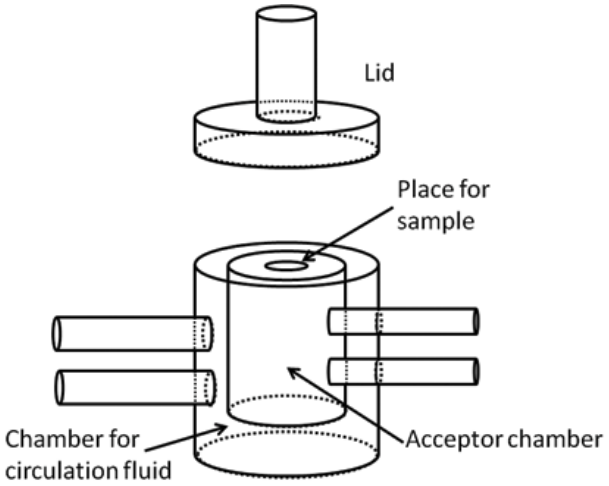

Figure 4.1: Diffusion cell

The use of a diffusion cell is a standard method for transdermal experiments. The usual procedure is to mount the skin, apply the chemical via the donor compartment, and then collect samples from the acceptor chamber at specific time intervals to obtain transdermal diffusion data. When the trial is complete, the skin is disposed of. In my research I have used the cells in a slightly different mode; the skin is mounted with the fluorophore solution and examined after 20 hours of diffusion, for performing optical microscopy.

Examining the skin in a microscope requires an imaging chamber. This consists of an object glass and a coverslip with extra padding to make sure the thick skin sample fits tightly between the glasses. The padding must to be thin enough to make sure the sample is in contact with the glass, to avoid airpockets, but it should also be thick enough to ensure that the sample is destroyed by too high pressure from the coverslip. Imaging chambers are commercially available, but are easy to make by applying double-coated adhesive tape to the coverslip.

4.1.2 Fresh tumour sample collection

The experiments in Paper III were performed on patients with histopathologically verified superficial basal cell carcinomas. The experiment was performed as a blind study, using MAL-cream (METVIX, Galderma, 160 mg/g methyl aminolevulinate as hydrochloride) and placebo cream (Unguentum M, Hermal Reinbek, Germany). Samples from three patients were used. MAL cream was applied to the lesions of two patients for 3 hours, and the placebo cream was applied to one lesion in the same manner. Biopsies were obtained from both the tumor bulk and perilesional normal skin. Half of the tissue biopsies obtained from one of the MAL treated patients were cryosectioned in 10 μm thin tissue sections and mounted on microscope slides, while the other half were stored in a freezer at -70° C. The full thickness skin biopsies were placed in an imaging chamber gasket with the skin surface against the cover glass and

mounted on a microscope slide. The slides with the prepared specimens were wrapped in aluminium foil to protect them from light, and stored in a freezer at -18° C for approximately 1 hour until imaging began.

4.1.3 Fluorophores

In Paper I, SRB was dissolved in PBS to a concentration of 3.4 μM and applied to the skin samples in the diffusion cell. In Paper II, RB and RBITC were dissolved in PBS to final concentrations of 100 nM for the skin experiments, and 200 nM for the reference measurements in solution. The concentrations were decided by trial and error, as no previous research protocol was available.

4.2 Gold nanoparticle gradient plates

The gradient plates were obtained from Cline Scientific AB (Gothenburg, Sweden). AuNPs of diameter 10 nm were deposited on the glass plates using an electrochemical method [110] and were ready to be used when delivered. A control reference, consisting of glass plates with the functionalization matrix (3-Aminopropyl)-diethyoxysilane (APDES) was given, also scanning electron microscopy data showing the concentration gradient. The gradient plates did not need any pre-treatment before using. They were placed in a custom made imaging chamber for the microscopy experiments. Between the experiments, they were kept in approximately 7° C in accordance with the manual.

4.3 The two photon microscopes

Two different microscopy systems were used in my work; one experimental setup and one commercial setup. The work in Papers I and II was performed on an experimental microscopy setup, where the laser and microscope are controlled manually. The uncovered laser beam path was aligned by using pinholes and an IR-viewer. The scanning was performed by scan mirrors controlled by a DOS program. Measurements in Papers III and IV were made with a commercial system, where the laser and the microscope are controlled and monitored by software. The entire setup was organized as a closed system, with no alignment or manual control required.

4.3.1 Experimental microscopy setup

The experimental setup used in Papers I and II consisted of a modified inverted Zeiss Axiovert 135 TV microscope, a BioRad MRC600 scan box, and two external GaAsP PMTs, see Figure 4.3. A 63x water immersion objective lens (Zeiss 'C-Apochromat' 63x/1.2 W Corr, working distance = 0.28 mm) was used for imaging and FCS. The scan mirrors within the scan box were used at a frequency of 512 Hz for the line galvanometer (x direction) and 1 Hz for the frame galvanometer(y direction). The excitation source, was a mode-locked femtosecond pulsed Tsunami Ti:sapphire laser, pumped by a Millennia Xs 10W diode-pump laser, with a maximum output power.

This laser has a wavelength output of 690 – 1080 nm, a repetition rate of 83 MHz, and a maximum output power of 10 W. The settings used were a wavelength of 840 nm and a pump power of 5 – 7 W, which gave an average output power of 700 –1000 mW. The power was controlled by a Pockels cell to a final average power at the sample of 0.5 – 25 mW. The pulse characteristics of the laser were measured with ALV software. The fluorescence intensity was binned and autocorrelated by an ALV-5000 Multiple Tau Digital Correlator acquisition card.

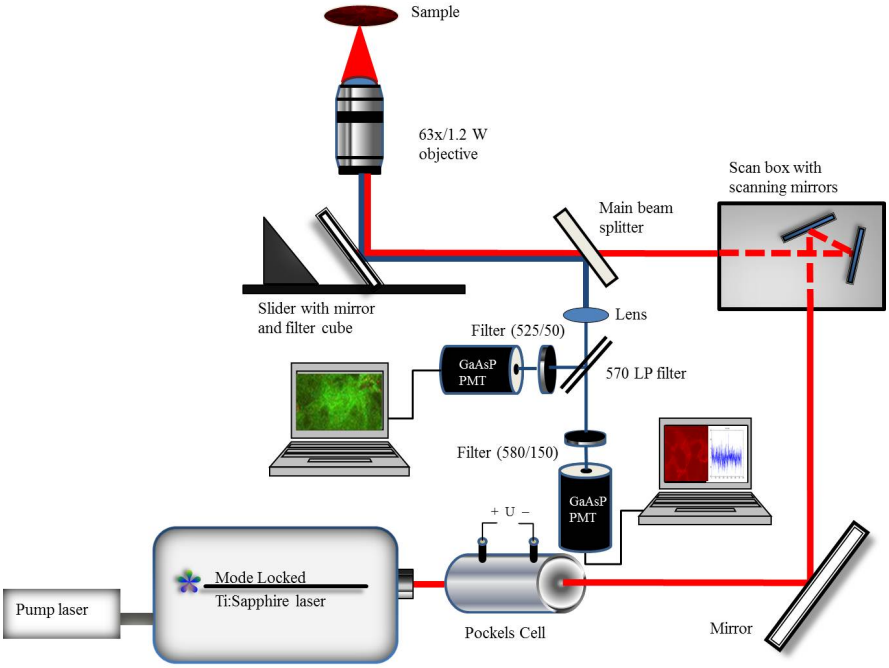

Figure 4.2: A schematic view over the experimental microscope setup.

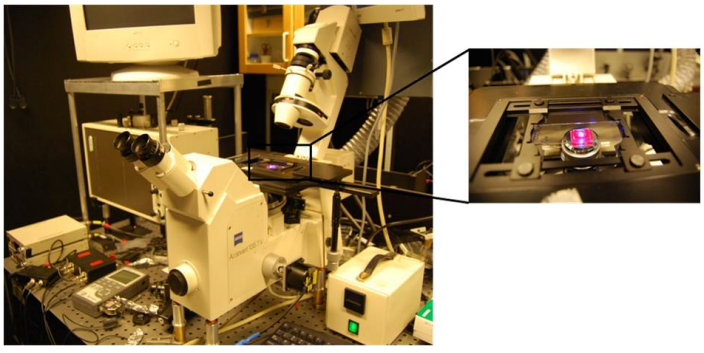

Figure 4.3: The experimental microscope setup. The insert shows a mounted skin sample, prepared for TPFCS.

4.3.2 Commercial microscopy setup

The work in Papers III and IV was performed with a commercial system: a Zeiss LSM 710 NLO equipped with a Mai Tai HP DeepSee laser, with a wavelength range of 690 – 1040 nm. The detection is performed by a 34-channel QUASAR detection unit. In front of the detector, there are prisms and slits, which makes it possible to select specific spectral regions without being restricted to certain filters, see figure 4.4 for an overview of the scan unit. This system is totally software controlled. The objective lens used was a 20x water immersion (Zeiss W Plan-Apochromat 20x/1.0) corrected for coverslips with a thickness of 0.17 mm. The working distance was 1.7 mm. The maximum output power is 3 W of the Mai Tai laser. The desired power at the sample is controlled by an AOM and chosen as percent of transmission, which was control measured for several percentage values. In general, powers of 30 – 100 mW were used.

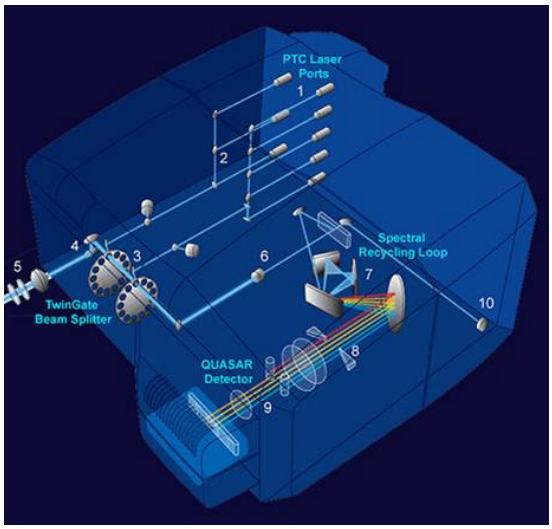

Figure 4.4: The interior of the scanning unit of the LSM710 system.

The scan unit of the commercial system is equipped with 1)laser ports for the visible lasers, 2)laser ports for IR-laser (the Mai Tai). The beam splitters in 3) are equipped with dichroic mirrors, one for each laser port, 4) is the scan mirrors, 5) is the exit from the scan unit to the microscope, and also the entrance for the emitted signal back into the scan unit. 6) is the pinhole for confocal scanning. 7) is a spectral recycling loop, which collects photons that becomes redirected by the grating. The prisms and slits used for wavelength selection is shown in 8), and 9) is the QUASAR detector. 10) is an exit for external detectors.

Chapter 5

Conclusions

The core of this thesis is the non-linear optics - the multiphoton microscope applied to biomedical studies, used in combination with correlation spectroscopy (Papers I and II) and as a single tool (Papers III and IV). This summary of five years of research provides a deeper knowledge of the appearance of non-linear processes and how they can be used in biomedical applications.

Measuring the diffusion, size, and colonization of molecules in human skin is of interest for the pharmaceutical industry, as topical delivery is a complementary method to oral intake and injections. It is also important for deeper understanding of contact allergy. The work presented in Papers I and II demonstrates a method which gives diffusion information. The diffusion, size, and localization of a reactive molecule show a probable location for the formation of allergen-protein conjugates. My results add to the existing qualitative reports of allergen-protein formation, giving a more complete picture of the allergen forming. This can lead to further research into isolating the specific proteins that the haptens bind to.

The measurements of the PSF in human skin were necessary for the diffusion analyses. These measurements were at different depths, from the surface down to 40 μm. Due to the high scattering properties of skin, it was expected that the PSF would become larger and more diffuse for deeper skin layers. However, the actual situation was the opposite; the PSF did not depend on the depth, but remained at the same size down to 40 μm. The PSF was measured as the FWHM of the intensity profile from sub-resolution fluorescent beads embedded in the excised skin samples. It was done for the lateral plane and the axial plane, and used for determine the focal volume in skin, which was used in the TPFCS analysis. The finding of the unchanged PSF has been reported before, by Dong *et al* [6], and later confirmed by Labouta *et al* and Durr *et al* [108, 111]. As a reference, PSF was measured on beads in solution, and the outcome was found to be similar to the measurements in skin. This implies that the distortions caused by the optical system are dominant over those in the skin.

The study in Paper III challenges previous research which suggests that multiphoton excitation with wavelengths around 780 nm of endogenously formed PpIX could give enhanced skin tumour contrast [17, 18, 112]. Although no conclusive evidence has been presented, the method is making its way into the clinics. We used spectral analy-

sis to demonstrate that two-photon excitation of endogenously formed PpIX does not provide additional contrast in superficial basal cell carcinomas. It was noticed that the PpIX signal was drowned in the autofluorescent background. The solution of slightly blue-shifting the excitation wavelength down to 710 nm gave a strong PpIX signal for the MAL-treated tumour sample, which is explained by an Anti-Stokes process. The small wavelength shift makes a huge difference to the excitation process, and would not cause any harm to the skin, as we are still in the optical window where the absorption is low. The result of this work can improve the diagnostics of skin cancers such as superficial basal cell carcinomas, which can save money, time and suffering for the patients.

The original idea of the research in paper IV was to investigate the penetration ability of AuNPs as these are good candidates for designing drug delivery methods. There are several reports stating that MIL signals from single AuNPs are not possible, but there are also reports claiming that MIL can identify single AuNPs. I used gradient plates, i.e. glass plates where 10 nm AuNPs were deposited in a concentration gradient. The most important finding was that MIL appears to require aggregation of the nanoparticles. Measurements on the gradient plates with 10 nm AuNPs gave a purely non-linear response, i.e. a slope value of 2, only at positions where the particles were clustered, which means cluster formation of at least two particles. It could also, in accordance with the findings of Paper III, be due to an anti-Stokes effect, which has previously been reported [93]. To clarify this, the band structure and corresponding probabilities and energies of the AuNPs has to be considered thoroughly. There are ongoing research of MIL of AuNPs in human skin [108] why further investigations are important.

Chapter 6

Outlook

The work presented in this thesis is far from finished, as many new questions have been raised. My plans for the future are to stay within this field as a post-doctoral researcher a and to contribute to future work with all the knowledge I have absorbed during my years as a PhD student. Some of my ideas are presented in this chapter.

The technique of two-photon microscopy has rapidly developed since its invention [5]; from being a pure laboratory tool, its use has been extended to the clinics as a complement in skin cancer diagnostics. Interesting future developments are for example nanoscopy, where the resolution is significantly increased [113]. Non-invasive multiphoton tomography is a concept from JenLab by König and co-workers in Saarbrüchen in Germany, where the autofluorescence is imaged by two-photon microscopy [114].

An interesting alternative to FCS is inverse-fluorescence correlation spectroscopy (iFCS). This is a new approach to diffusion measurements, with the first publication having come from Wennmalm *et al.* in 2009. Instead of measuring the signal from the particles of interest, the method measures the signal from the surroundings. This requires a high signal to background ratio. The main benefit of iFCS is that the particles are left intact which minimizes the risk of influence from any labelling fluorophore. This method might be the solution to the problem of measuring diffusion *in vivo*, and may be able to reveal information not available today.

Another interesting FCS alternative is the technique of fluorescence triple correlation spectroscopy (F3CS), as reported by Ridgeway *et al.* [115]. The idea is to divide the emitted signal and collect it with three different PMTs. The triple correlation function gives better statistics and noise from a single PMT will be averaged out. This method is a good candidate for overcoming the ever-present noise in human skin.

In my research I have used a data acquisition card for the FCS analysis, which bins the data and then performs the correlation analyse. The output achieved from this card is the binned data and the ready correlated data, there is no possibility of getting access to the full raw data, i.e. the fluorescence signal without the binning. The modern acquisition cards available today has a better time-resolution and should give the user more insight in the fluorescence signal. It could also be interesting to do TCSPC fluorescence lifetime imaging (FLIM) [116].

I have used different fluorophores for measuring the diffusion with TPFCS. It could also be of interest to use AuNPs for this purpose, previously tried by Wang *et al.* using gold nanorods [117]. Interestingly, the FCS analysis performed by Wang *et al.* revealed that the rods were twice as large as expected from the manufacturing. The authors explained this as being a result of the PEGylated surface of the rods, but it might also imply that the rods have aggregated. This technique might allow investigation not only of the diffusion coefficient, but also of the clustering tendency of AuNPs in skin.

Performing long-term measurements when using a water immersion objective lens can be problematic due to the evaporation of the water. An alternative is to use an oil immersion objective lens, which has the advantage of providing higher NA. However, as skin has a high water content, the oil would introduce an undesirable change in refractive index. Instead, longer measurements could be enabled by retaining the water immersion objective lens and putting a thin latex tube around it to prevent evaporation.

Acknowledgements

I would like to thank several people who all have contributed to this thesis.

First of all, I would like to express my deepest gratitude to my supervisor Marica B. Ericson for guiding me into the interesting cross section of physics and biology. You are an inspiration and a role model and you possess what seems like an infinite source of patience!

Many thanks to Dag Hanstorp for all your valuable input in my work and for being my examinor. Thanks to my assistant supervisor Maria Smedh and Mattias Goksör for taking your time and for teaching me the noble art of doing research and writing papers.

Many thanks to the present and past members in the Biomedical photonics group: Vladimir Kirejev, Johan Borglin, Yuanmo Wang and Brigitte Bauer.

Despina Kantere and Hanne Evenbratt. How boring life at the microscope would have been without you! Thanks for guiding me through the chemistry and medical part of my work!

Thanks to all the members at the Dermatochemistry Department at the University of Gothenburg, especially Carl Simonsson for sharing your lab equipment as well as your chemistry knowledge, and for letting me use your skin illustrations. Thanks also to the Department of Dermatology at Sahlgrenska University Hospital, Gothenburg especially Christina Halldin for spending your time with collection and preparations of skin sample.

The members of the former Physics Level 6 and the present Physics Level 8; you are great! Thanks for interesting and fruitful discussions about life in general and science in particular.

Thanks to my father Lars Guldbrand for encouraging me to a higher education, and for believing in me. Thanks to all of my friends, especially the closest: Bums, Carina, Helén, Loois and Nina.

And Michael for your love ♡.

Bibliography

[1] M. Göppert-Mayer. Über Elementarakte mit zwei Quantensprüngen. *Annalen der Physik*, 9:273–295, 1931.

[2] Barry R. Masters and Peter T. C. So. *Handbook of biomedical nonlinear optical microscopy*. Oxford University Press, Inc, 198 Madison Avenue, New York, New York 10016, 2008.

[3] W. Kaiser and C. G. B. Garrett. Two-photon Excitation in CaF_2:Eu^{2+}.

[4] W. Denk and K. Svoboda. Photon upmanship: Why multiphoton imaging is more than a gimmick. *Neuron*, 18:351–357, 1997.

[5] W. Denk, J. H. Strickler, and W. W. Webb. Two photon laser scanning fluorescence microscopy. *Science*, 248(4951):73–76, 1990.

[6] C. Y. Dong, K. König, and P. T. C. So. Characterizing point spread functions of two-photon fluorescence microscopy in turbid medium. *Journal of Biomedical Optics*, 8(3):450–459, 2003.

[7] P. T. C. So, C. Y. Dong, B. R. Masters, and K. M. Berland. Two-photon excitation fluorescence microscopy. *Annual Review of Biomedical Engineering*, 2:399–429, 2000.

[8] W. R. Zipfel, R. M. Williams, and W. W. Webb. Nonlinear magic: multiphoton microscopy in the biosciences. *Angewandte Chemie*, 50:5274–5293, 2011.

[9] K. König. Multiphoton microscopy in life sciences. *Journal of Microscopy-Oxford*, 200:83–104, 2000.

[10] B. R. Masters, P. T. C. So, and E. Gratton. Multiphoton excitation fluorescence microscopy and spectroscopy of in vivo human skin. *Biophysical Journal*, 72(6):2405–2412, 1997.

[11] K. König and I. Riemann. High-resolution multiphoton tomography of human skin with subcellular spatial resolution and picosecond time resolution. *Journal of Biomedical Optics*, 8(3):432–439, 2003.

[12] B. R. Masters, P. T. C. So, and E. Gratton. Multiphoton excitation microscopy of in vivo human skin - functional and morphological optical biopsy based on three-dimensional imaging, lifetime measurements and fluorescence spectroscopy. *Advances in Optical Biopsy and Optical Mammography*, 838:58–67, 1998.

[13] B. Yu, C. Y. Dong, P. T. C. So, D. Blankschtein, and R. Langer. In vitro visualization and quantification of oleic acid induced changes in transdermal transport using two-photon fluorescence microscopy. *Journal of Investigative Dermatology*, 117(1):16–25, 2001.

[14] J. Bender, C. Simonsson, M. Smedh, S. Engström, and M. B. Ericson. Lipid cubic phases in topical drug delivery: Visualization of skin distribution using two-photon microscopy. *Journal of Controlled Release*, 129(3):163–169, 2008.

[15] J. Paoli, M. Smedh, A. M. Wennberg, and M. B. Ericson. Multiphoton laser scanning microscopy on non-melanoma skin cancer: Morphologic features for future non-invasive diagnostics. *Journal of Investigative Dermatology*, 128(5):1248–1255, 2008.

[16] E. Dimitrow, M. Ziemer, M. J. Koehler, J. Norgauer, K. König, P. Elsner, and M. Kaatz. Sensitivity and specificity of multiphoton laser tomography for in vivo and ex vivo diagnosis of malignant melanoma. *Journal of Investigative Dermatology*, 129(7):1752–1758, 2009.

[17] K. König, A. P. Raphael, L. Lin, J. E. Grice, H. P. Soyer, H. G. Breunig, M. S. Roberts, and T. W Prow. Applications of multiphoton tomographs and femtosecond laser nanoprocessing microscopes in drug delivery research. *Advanced Drug Delivery Reviews*, 63(4-5):388–404, 2011.

[18] R. Cicchi, S. Sestini, V. De Giorgi, T. Lotti, and F. S. Pavone. Nonlinear laser imaging of skin lesions. *Journal of Biophotonics*, 1(1):62–73, 2008.

[19] R. A. Sperling, R. R. Gil, F. Zhang, M. Zanella, and W. J. Parak. Biological applications of gold nanoparticles. *Chemical Society Review*, 37:1896–1908, 2008.

[20] M-C. Daniel and D. Astruc. Gold nanoparticles: Assembly, supramolecular chemistry, quantum-size-related properties, and applications toward biology, catalysis, and nanotechnology. *Chemical Reviews*, 104(1):293–346, 2004.

[21] D-R. Chen, C. H. Wendt, and D. Y. H. Pui. A novel approach for introducing bio-materials into cells. *Journal of Nanoparticle Research*, 2:133–139, 2000.

[22] J. Chen, B. Wiley, Z-Y. Li, D. Campbell, F. Saeki, H. Cang, L. Au, J. Lee, X. Li, and Y. Xia. Gold nanocages: Engineering their structure for biomedical applications. *Advanced Materials*, 17:2255–2261, 2005.

[23] X. Huang, I. H. El-Sayed, W. Qian, and M. A. El-Sayed. Cancer cell imaging and photothermal therapy in the near-infrared region by using gold nanorods. *Journal of American Chemical Society*, 128:2115 – 2120, 2006.

[24] D. Pissuwan, S. M. Valenzuela, and M. B. Cortie. Therapeutic possibilities of plasmonic heated gold nanoparticles. *Trends in Biotechnology*, 24(2):62–67, 2006.

[25] J. Park, A. Estrada, K. Sharp, K. Sang, J. A. Schwartz, D. K. Smith, C. Coleman, J. D. Payne, B. A. Korgel, A. K. Dunn, and J. W. Tunnell. Two-photon-induced photoluminescence imaging of tumors using near-infrared excited gold nanoshells. *Optics Express*, 16(3):1590–1599, 2008.

[26] William J Croft. *Under the Microscope, A Brief History of Microscopy.* World Scientific Publishing Co. Pte. Ltd, 2006.

[27] Joseph R. Lakowicz. *Principles of Fluorescence Spectroscopy.* Springer Science + Business Media, LLC, 233 Spring Street, New York, NY 10013, USA, 2006.

[28] O. Axner. *Analysis and Design of Optical Systems.* 2009.

[29] Francis A. Jenkins and Harvey E. White. *Fundamentals of Optics.* McGraw-Hill, Inc., 1976.

[30] Barry R. Masters. *Confocal Microscopy and Multiphoton Excitation Microscopy, The Genesis of Live Cell Imaging.* SPIE - The International society for Optical Imaging, P.O. Box 10, Bellingham, Washington 98227 - 0010 USA, 2006.

[31] http://www.olympusmicro.com/primer/anatomy/specifications.html.

[32] P. Schwille and E. Haustein. Fluorescence correlation spectroscopy, an introduction to its concepts and applications. *Biophysics Textbook Online (BTOL)*, pages 1–33, 2004.

[33] D. T. Craggs. Green fluorescent protein: structure, folding and chromophore maturation. *Chemical Society Reviews*, 38(10):2865–2875, 2009.

[34] K. Samuelsson, C. Simonsson, C. A. Jonsson, G. Westman, M. B. Ericson, and A-T. Karlberg. Accumulation of fitc near stratum corneum-visualizing epidermal distribution of a strong sensitizer using two-photon microscopy. *Contact Dermatitis*, 61(2):91–100, 2009.

[35] N.S. Claxton, T.J. Fellers, and M. W. Davidson. Laser scanning confocal microscopy. Department of Optical Microscopy and Digital Imaging, National High Magnetic Field Laboratory, The Florida State University, Tallahassee, Florida 32310, http://www.olympusfluoview.com.

[36] Eugene Hecht. *Optics.* Addison-Wesley Longman, Inc., Adelphi University, New York, NY, 2002.

[37] Carl Nordling and Jonny Österman. *Physics Handbook for Science and Engineering.* Studentlitteratur, Lund, Sweden, 1999.

[38] P. A. Franken, A. E. Hill, C. W. Peters, and G. Weinreich. Generation of optical harmonics. *Physical Review Letters*, 7(4):118–120, 1977.

[39] R. Gauderon, P. B. Lukins, and C. J. R. Sheppard. Optimization of second-harmonic generation microscopy. *Micron*, 32:691–700, 2001.

[40] J. Chen, S. Zhuo, T. Luo, X. Jiang, and J. Zhao. Spectral characteristics of autofluorescence and second harmonic generation from ex vivo human skin induced by femtosecond laser and visible lasers. *Scanning*, 28:319–326, 2006.

[41] G. Chen, J. Chen, S. Zhuo, S. Xiong, H. Zeng, X. Jiang, R. Chen, and S. Xie. Nonlinear spectral imaging of human hypertrophic scar based on two-photon excited fluorescence and second-harmonic generation. *British Journal of Dermatology*, 161:48–55, 2009.

[42] R. Cicchi, D. Kapsokalyvas, V. De Giorgi, V. Maio, A. Van Wiechen, D Massi, T. Lotti, and F. S. Pavone. Scoring of collagen orgainzation in healthy and diseased human dermis by multiphoton microscopy. *Journal of Biophotonics*, 3(1-2):34–43, 2010.

[43] J. Cheng and X. S. Xie. Coherent anti-stokes raman scattering microscopy: Instrumentation, theory, and applications. *J. Phys. Chem. B*, 108:827–840, 2004.

[44] M. Müller and A. Zumbusch. Coherent anti-stokes raman scattering microscopy. *ChemPhysChem*, 8:2156–2170, 2007.

[45] A. Volkmer. Vibrational imaging and microspectroscopies based on coherent anti-stokes raman scattering microscopy. *Journal of Physics D: Applied Physics*, 38:R59–R81, 2005.

[46] O. Burkacky, A. Zumbusch, C. Brackmann, and A. Enejder. Dual-pump coherent anti-stokes-raman scattering microscopy. *Optics Letters*, 31(24):3656–3658, 2006.

[47] V. E. Centonze and J. G. White. Multiphoton excitation provides optical sections from deeper within scattering specimens than confocal imaging. *Biophysical Journal*, 75:2015–2024, 1998.

[48] http://www.rp-photonics.com/encyclopedia.html.

[49] D. Magde, E. L. Elson, and W. W. Webb. Thermodynamic fluctuations in a reacting system - measurement by fluorescence correlation spectroscopy. *Physical Review Letters*, 29(11):705–708, 1972.

[50] H. Qian, L. Elliot Elson, and C. Frieden. Studies on the structure of actin gels using time correlation spectroscopy of fluorescent beads. *Biophysical Journal*, 63:1000–1010, 1992.

[51] P. F. Fahey, D. E. Koppel, L. S. Barak, D. E. Wolf, E. L. Elson, and W. W. Webb. Lateral diffusion in planar lipid bilayers. *Science*, 195:305–306, 1977.

[52] K. M. Berland, P. T. C. So, Y. Chen, W. W. Mantulin, and E. Gratton. Scanning two-photon fluctuation correlation spectroscopy: Particle counting measurements for detection of molecular aggregation. *Biophysical Journal*, 71:410–420, 1996.

[53] A. G. Palmer and N. L. Thompson. Molecular aggregation characterized by high order autocorrelation in fluorescence correlation spectroscopy. *Biophysical Journal*, 52:257–270, 1987.

[54] P. Schwille, U. Haupts, S. Maiti, and W. W. Webb. Molecular dynamics in living cells observed by fluorescence correlation spectroscopy with one- and two-photon excitation. *Biophysical Journal*, 77(4):2251–2265, 1999.

[55] P. Schwille, J. Korlach, and W. W. Webb. Fluorescence correlation spectroscopy with single-molecule sensitivity on cell and model membranes. *Cytometry*, 36:176–182, 1999.

[56] K. M. Berland, P. T. C. So, and E. Gratton. Two-photon fluorescence correlation spectroscopy: Method and application to the intracellular environment. *Biophysical Journal*, 68:694–701, 1995.

[57] Z. Wang, J. V. Shah, Z. Chen, C-H. Sun, and M. W. Berns. Fluorescence correlation spectroscopy investigation of a gfp mutant-enhanced cyan fluorescent protein and its tubulin fusion in livin cells with two-photon excitation. *Journal of Biomedical Optics*, 9(2):395–403, 2004.

[58] G. Alexandrakis, E. B. Brown, R. T. Tong, T. D. McKee, R. B. Campbell, Y. Boucher, and R. K. Jain. Two-photon fluorescence correlation microscopy reveals the two-phase nature of transport in tumors. *Nature Medicine*, 10(2):203–207, 2004.

[59] C. R. Daniels, L. Kisley, H. Kim, W-H. Chen, M-V. Poongavanam, C. Reznik, K. Kourentzi, R. C. Willson, and C. F. Landes. Fluorescence correlation spectroscopy study of protein transport and dynamic interactions with clustered-charge peptide adsorbents. *Journal of Molecular Recognition*, 25:435–442, 2012.

[60] S. Ranjit and M. Levitus. Probing the interaction between fluorophores and dna nucleotides by fluorescence correlation spectroscopy and fluorescence quenching. *Photochemistry and Photobiology*, 88:782 – 791, 2012.

[61] J. Wang, X. Huang, F. Zan, C. Guo, C. Cao, and J. Ren. Studies on bioconjugation of quantum dots using capillary electrophoresis and fluorescence correlation spectroscopy. *Electrophoresis*, 33:1987–1995, 2012.

[62] C. Dong and J. Irudayaraj. Hydrodynamic size-dependent cellular uptake of aqueous qds probed by fluorescence correlation spectroscopy. *The Journal of Physical Chemistry B*, 116:12125–12132, 2012.

[63] Charles Kittel. *Introduction to Solid State Physics*. John Wiley & Sons, Inc, 7th edition, New York, USA, 1996.

[64] Franz Mandl. *Statistical Physics*. John Wiley & Sons, Ltd., 1988.

[65] M.A. Islam. Fickian diffusion equation - an unsolved problem. *Physica Scripta*, 70:114–119, 2004.

[66] J. Ries and P. Schwille. Fluorescence correlation spectroscopy. *Bioessays*, 34:361–368, 2012.

[67] N. Bag, J. Sankaran, A. Paul, R. S. Kraut, and T. Wohland. Calibration and limits of camera-based fluorescence correlation spectroscopy: A supported lipid bilayer study. *ChemPhysChem*, 13:2784–2794, 2012.

[68] Y. Ohsugi and M. Kinjo. Multipoint fluorescence correlation spectroscopy with total internal reflection fluorescence microscope. *Journal of Biomedical Optics*, 14(1):014030–1 – 01430–4, 2009.

[69] W. Becker. Fluorescence lifetime imaging - techniques and applications. *Journal of Microscopy*, 247:119–136, 2012.

[70] Gerard J. Tortora and Sandra Reynolds. Grabowski. *Introduction to the human body*. John Wiley & Sons, Inc., 605 Third Avenue, New York, NY, 2001.

[71] A-T. Karlberg, M. A. Bergström, A. Börje, K. Luthman, and J. L. G. Nilsson. Allergic contact dermatitis - formation, structural requirements and reactivity of skin sensitizers. *Chemical Research in Toxicology*, 21:53–69, 2008.

[72] S. J. Miller. Etiology and pathogenesis of basal cell carcinoma. *Clinics in Dermatiology*, 13:527–536, 1995.

[73] K. Kalka, H. Merk, and H. Mukhtar. Photodynamic therapy in dermatology. *Journal of the American Academy of Dermatology*, 42(3):389–413, 2000.

[74] J. Hadgraft. Skin, the final frontier. *International Journal of Pharmaceutics*, 224(1-2):1–18, 2001.

[75] A. N. Bashkatov, E. A Genina, V. I. Kochubey, and V. V. Tuchin. Optical properties of human skin, subcutaneous and mucous tissues in the wavelength range from 400 to 2000 nm. *Journal of Physics D: Applied Physics*, 38:2543–2555, 2005.

[76] Ashley J. Welch and Martin J.C. van Gemert. *Optical-thermal response of laser-irradiated tissue*. Plenum Press, New York, 1995.

[77] S. Huang, A. A. Heikal, and W. W. Webb. Two-photon fluorescence spectroscopy and microscopy of nad(p)h and flavoprotein. *Biophysical Journal*, 82:2811–2825, 2002.

[78] H. H. Bragulla and D. G. Homberger. Structure and functions of keratin proteins in simple, stratified, keratinized and cornified epithelia. *Journal of Anatomy*, 214:516–559, 2009.

[79] Y. Yu, A. M. D. Lee, H. Wang, S. Tang, J. Zhao, H. Lui, and H. Zeng. Imaging-guided two-photon excitation-emission-matrix measurements of human skin tissues. *Journal of Biomedical Optics*, 17(7):0770041 – 0770048, 2012.

[80] K. Schenke-Layland, I. Riemann, O. Damour, U. A. Stock, and K. König. Two-photon microscopes and *in vivo* multiphoton tomographs - powerful diagnostic tools for tissue engineering and drug delivery. *Advanced Drug Delivery Reviews*, 58(7):878–896, 2006.

[81] X. Han, H. Lui, D. I. McLean, and H. Zeng. Near-infrared autofluorescence imaging of cutaneous melanins and human skin *in vivo*. *Journal of Biomedical Optics*, 14(2):024017–1 – 024017–5, 2009.

[82] M. B. Ericson, C. Simonsson, S. Guldbrand, C. Ljungblad, J. Paoli, and M. Smedh. Two-photon laser-scanning fluorescence microscopy applied for studies of human skin. *Journal of Biophotonics*, 1(4):320–330, 2008.

[83] J. Ying, F. Liu, and R. R. Alfano. Effect of scattering on nonlinear optical scanning microscopy imaging of highly scattering media. *Applied Optics*, 39(4):509–514, 2000.

[84] H. G. Breunig, H. Studier, and K. König. Multiphoton excitation characteristics of cellular fluorophores of human skin in vivo. *Optics Express*, 18(8):7857–7871, 2010.

[85] A-T. Karlberg, D. Basketter, A. Goossens, and J-P. Lepoittevin. Regulatory classification of substances oxidized to skin sensitizers on exposure to air. *Contact Dermatitis*, 40:183–188, 199.

[86] J. C. Kennedy, R. H. Pottier, and D. C. Pross. Photodynamic therapy with endogenous protoporphyrin IX: basic principles and present clinical experience. *Journal of Photochemistry and Photobiology, B:Biology*, 6:143–148, 1990.

[87] B. Stenquist, M. B. Ericson, C. Strandeberg, L. Mölne, A. Rosén, O. Larkö, and A. M. Wennberg. Bispectral fluorescence imaging of aggressive basal cell carcinoma combined with histopathological mapping: a preliminary study indicating a possible adjunt to mohs micrographic surgery. *Brittish Journal of Dermatology*, 154:305–309, 2005.

[88] C. J. Murphy, A. M. Gole, J. W. Stone, P. N. Sisco, A. M. Alkilany, E. C. Goldsmith, and S. C. Baxter. Gold nanoparticles in biology: Beyond toxicity to cellular imaging. *Accounts of Chemical Research*, 41(12):1721–1730, 2008.

[89] http://www.webexhibits.org/causesofcolor/9.html.

[90] T. Gosh, S. K. Pal. Interparticle coupling effect on the surface plasmon resonance of gold nanoparticles: From theory to applications. *Chemical Reviews*, 107:4797–4862, 2007.

[91] Travis Jennings and Geoffrey Strouse. *Past, Present, and Future of Gold Nanoparticles, Advances in Experimental Medicine and Biology.* Landes Bioscience and Springer Science + Business Media, 2007.

[92] G. T. Boyd, Z. H. Yu, and Y. R. Shen. Photoinduced luminescence from the noble metals and its enhancement on roughened surfaces. *Physical Review B*, 33(12):7923–7936, 1986.

[93] M. R. Beversluis, A. Bouhelier, and L. Novotny. Continuum generation from single gold nanostructures through near-field mediated intraband transitions. *Physical Review B*, 68:1154331–11543310, 2003.

[94] K. Imura, T. Nagahara, and H. Okamoto. Plasmon mode imaging of single gold nanorods. *Journal of American Chemical Society Communications*, 126:12730–12731, 2004.

[95] T. G. Schaaff, N. Shafigullin, J. T. Khoury, I. Vezmar, R. L. Whetten, W. G. Cullen, P. N. First, C. Gutiérrez-Wing, J. Ascensio, and M. J. Jose-Yacamán. Isolation of smaller nanocrystal au molecules: Robust quantum effects in optical spectra. *Journal of Physical Chemistry B*, 101:7885–7891, 1997.

[96] A. Mooradian. Photoluminescence of metals. *Physical Review Letters*, 22(5):185–187, 1969.

[97] K. Imura, T. Nagahara, and H. Okamoto. Near-field two-photon-induced photoluminescence from single gold nanorods and imaging of plasmon modes. *Journal of Physical Chemiistry B*, 109:13214–13220, 2005.

[98] J. Kimling, M. Maier, V. Okenve, H. Kotaidis, H. Ballot, and A. Plech. Turkevich method for gold nanoparticle synthesis revisited. *Journal of Physical Chemistry B*, 110:15700–15707, 2006.

[99] M. Brust, M. Walker, D. Bethell, D. J Schiffrin, and R. Whyman. Synthesis of thiol-derivatised gold nanoparticles in a two-phase liquid-liquid system. *Journal of the Chemical Society-Chemical Communications*, (7):801–802, 1994.

[100] J. Turkevich, P. C. Stevenson, and J. Hillier. A study of the nucleation and growth processes in the synthesis of colloidal gold. *Faraday Discussion Society*, 11:55–75, 1951.

[101] G. Frens. Controlled nucleation for the regulation of the particle size in monodisperse gold suspensions. *Nature*, 241:20–22, 1973.

[102] Y-K. Hong, K. Hanchul, G. Lee, W. Kim, J-I. Park, J. Cheon, and J-Y. Koo. Controlled two-dimensional distribution of nanoparticles by spin-coating method. *Applied Physics Letters*, 80(5):844–846, 2002.

[103] L. Wang, W. Mao, D. Ni, J. Di, Y. Wu, and Y. Tu. Direct electrodeposition of gold nanoparticles onto indium/tin oxide film coated glass and its application for electrochemical biosensor. *Electrochemistry Communications*, 10:673–676, 2008.

[104] B. Bauer, S. Chen, M. Käll, L. Gunnarsson, and M. B. Ericson. Metal nanoparticles amplify photodynamic effect on skin cells in vitro. *Proceedings of SPIE*, 7897:7897121–7897128, 2011.

[105] P. K. Jain, I. H. El-Sayed, and M. A. El-Sayed. Au nanoparticles target cancer. *Nanotoday*, 2(1):18–29, 2007.

[106] N. J. Durr, T. Larson, D. K. Smith, B. A. Korgel, K Sokolov, and A. Ben-Yakar. Two-photon luminescence imaging of cancer cells using molecularly targeted gold nanorods. *Nano Letters*, 7(4):941–945, 2007.

[107] N. K. Balla, C. J. R. Sheppard, and P. T. C. So. Multiphoton luminescence of gold nanorods upon excitation with wavelengths away from their absorption maxima. *Proceedings of SPIE*, 7910:79100N1–79100N6, 2011.

[108] H. I. Labouta, M. Hampel, S. Thude, K. Reutlinger, K.-H. Kostka, and M. Schneider. Depth profiling of gold nanoparticles and characterization of point spread functions in reconstructed and human skin using multiphoton microscopy. *Journal of Biophotonics*, 5(1):85–96, 2012.

[109] W. J. Addicks, G. L. Flynn, and N. Weiner. Validation of a flow-through diffusion cell for use in transdermal research. *Pharmaceutical Research*, 4(4):337–341, 1987.

[110] H. Elwing, S. Welin, A. Askendal, U. Nilsson, and I. Lundström. A wettability gradient method for studies of macromolecular interactions at the liquid/solid interface. *Journal of Colloid and Interface Science*, 119(1):203–210, 1987.

[111] N. J. Durr, C. T. Weisspfennig, B. A. Holfeld, and A. Ben-Yakar. Maximum imaging depth of two-photon autofluorescence microscopy in epithelial tissues. *Journal of Biomedical Optics*, 16(2):0260081–02600813, 2011.

[112] I. Riemann, A. Ehlers, D. Dill-Müller, S. Martin, and K. König. Multiphoton tomography of skin tumors after ala application. *Proc. of SPIE*, 6424:642405–1 – 642405–6, 2007.

[113] S.W. Hell. Far-field optical nanoscopy. *Science*, 316:1153–1158, 2007.

[114] K. König. Clinical multiphoton tomography. *Journal of Biophotonics*, 1(1):13–23, 2008.

[115] W. K. Ridgeway, D. P. Millar, and J. R. Williamson. The spectroscopic basis of fluorescence triple correlation spectroscopy. *The Journal of Physical Chemistry B*, 116:1908 – 1919, 2011.

[116] S. Kumar, C. Dunsby, P. A. A. De Beule, D. M. Owen, U. Anand, P. M. P. Lanigan, R. K. P. Benninger, D. M. Davis, M. A. A. Neil, P. Anand, C. Benham, A. Naylor, and P. M. W. French. Multifocal multiphoton excitation and time correlated single photon counting detection for 3-d fluorescence lifetime imaging. *Optics Express*, 15(20):12548–12561, 2007.

[117] H. Wang, T. B. Huff, D. A. Zweifel, W. He, P. S. Low, A. Wei, and J.-X. Cheng. In vitro and in vivo two-photon luminescence imaging of single gold nanorods. *Proceedings of the National Academy of Sciences of the United States of America*, 102(44):15752–15756, 2005.